

In presenting the dissertation as a partial fulfillment of the requirements for an advanced degree from the Georgia Institute of Technology, I agree that the Library of the Institute shall make it available for inspection and circulation in accordance with its regulations governing materials of this type. I agree that permission to copy from, or to publish from, this dissertation may be granted by the professor under whose direction it was written, or, in his absence, by the Dean of the Graduate Division when such copying or publication is solely for scholarly purposes and does not involve potential financial gain. It is understood that any copying from, or publication of, this dissertation which involves potential financial gain will not be allowed without written permission.

John Paul Kame

3/17/65

b

STUDIES OF THE M/L ORBITAL ELECTRON CAPTURE RATIO
IN AR³⁷ DECAY

A THESIS

Presented to

The Faculty of the Graduate Division

by

Jean-Paul A. Renier

In Partial Fulfillment

of the Requirements for the Degree

Master of Science in Nuclear Engineering

Georgia Institute of Technology

June, 1967

STUDIES OF THE M/L ORBITAL ELECTRON CAPTURE RATIO
IN AR³⁷ DECAY

BOUND BY THE NATIONAL LIBRARY BINDERY CO. OF GA.

Approved:

R.W. Fink

Chairman

B. Eichholz

C. J. Roberts

Date approved by Chairman: **MAY 31 1967**

ACKNOWLEDGMENTS

The author wishes to thank Dr. K. W. D. Ledingham and the author's thesis adviser, Professor R. W. Fink, for suggesting this problem and for helpful advice. To his friend and co-worker, Mr. H. D. Genz, the author wishes to express his indebtedness for friendly collaboration on orbital capture studies. The author appreciates the counsel of Professor J. C. Clement as his faculty adviser. Thanks are due Mrs. Lydia S. Geeslin for typing this thesis. Finally, the author thanks the U. S. Atomic Energy Commission for financial support of this research through contract number AT(40-1)-3346.

TABLE OF CONTENTS

	Page
ACKNOWLEDGMENTS	ii
LIST OF TABLES.	iv
LIST OF ILLUSTRATIONS	v
SUMMARY	vi
Chapter	
I. INTRODUCTION	1
Theoretical Considerations for Allowed Transitions	
Comparison of Theory and Previous Experimental Results	
Choice of a Low-Z Nuclide: Ar^{37}	
The K-, L-, and M-Spectra in Ar^{37} Decay	
II. EXPERIMENTAL MEASUREMENTS.	16
Preparation and Handling of Radioactive Ar^{37} Source	
Description of Single-wire Proportional Counter	
Gas Filling	
Electronic System	
Afterpulses in Proportional Counters	
Single-electron Spectroscopy	
Energy Calibrations, Optimization for the Ar^{37}	
Spectrum, and System Stability	
Experimental Measurements	
III. RESULTS.	38
Data and Computation of Observed L/K and M/L	
Intensity Ratios	
Correction for K X-ray Escape and Calculation	
of Final Results	
Evaluation of Experimental Errors	
The Capture Ratio, P_M/P_L , as a Function of k_α	
IV. DISCUSSION OF RESULTS.	49
BIBLIOGRAPHY.	51

LIST OF TABLES

Table	Page
1. Observed M/L Intensity Ratios, Uncorrected for K X-ray Escape	40

LIST OF ILLUSTRATIONS

Figure	Page
1. Comparison of Experimental M/L Orbital Electron Capture Ratios with Theoretical Results.	11
2. Counter Construction and RC High Voltage Smoothing Filters.	17
3. Block Diagram of Electronic Detection System	19
4. Block Diagram of Paralysis Pulse Generator	22
5. Circuit Diagram of Paralysis Pulse Generator	23
6. Pulse Sequence Diagram of Paralysis Pulse Generator. . .	25
7. Modification of Linear Anticoincidence Gate to Produce Zero Time Recovery	26
8. Ar ³⁷ M-spectrum as a Function of Paralysis Pulse Width.	32
9. Spectrum of Ar ³⁷ K-peak.	35
10. Ar ³⁷ M + L Composite Spectrum and Background Shape . . .	36
11. Ar ³⁷ M-spectrum with Single-electron Shape and Background Spectrum.	37
12. Plot of (P_M/P_L) Capture Ratio versus k_α	48

SUMMARY

Recent investigations of the pulse height distribution from proportional counters due to single- and multiple-electron events make it possible to measure single electron spectra down to essentially zero energy with much greater accuracy than heretofore. The ratio of M- to L-orbital electron capture in the decay of 35-day Ar^{37} has been measured in a single-wire proportional counter containing the gaseous source. This counter was operated with variable paralysis times, 3.8 milliseconds being used in the present experiments to minimize the contribution from negative ions. The experiment was undertaken because of the considerable disagreement between experimental and theoretical M/L capture ratios, particularly in the region of low Z. A survey of all experimental work on M-capture is included for comparison with available theoretical results.

The experimental result for the M/L capture ratio in Ar^{37} decay can be expressed as a function of k_α , the function of K_α x-rays in the K x-ray series of chlorine ($Z = 17$), in the following typical equation (valid for one atmosphere counter pressure with argon-propane filling).

$$(P_M/P_L) = 0.0714 + 0.500 \left[\frac{1.0714 k_\alpha - 1}{k_\alpha + 0.153} \right]$$

From experiments carried out at one and two atmospheres counter pressure, limits on the values of k_α and (P_M/P_L) can be set as follows:

$$k_{\alpha} > 0.95 \quad \text{and} \quad 0.085 \leq P_M/P_L \leq 0.105$$

From these limits, which include probable errors, a clear disagreement has been established between the experimental M/L orbital electron capture ratio in Ar^{37} decay and exchange-corrected theory. This disagreement, which is much more pronounced for M/L- than for L/K-capture ratios, may arise from screening assumptions contained in the Hartree-Fock wave functions of Watson and Freeman.

CHAPTER I

INTRODUCTION

Orbital electron capture by the nucleus is one of four possible modes of beta decay in which the total number of nucleons does not change. Beta transitions are characterized by the transformation of neutrons into protons and vice versa, with emission or capture of leptons and/or neutrinos, with conservation of energy, charge, momenta, and spin. These four basic transformations are:

1. β^- decay: $\langle n \rangle \approx \langle p \rangle + \beta^- + \bar{\nu}$
(anti-neutrino)
2. β^+ decay: $\langle p \rangle \approx \langle n \rangle + \beta^+ + \nu$
(neutrino)
3. Orbital electron capture (EC): $\langle p \rangle + e_i^- \approx \langle n \rangle + \nu$
(monoenergetic-neutrino)
(for capture of an electron bound in the i-th atomic shell)
4. e^+ capture: $\langle n \rangle + e^+ \approx \langle p \rangle + \nu$
(neutrino)
(This process has not yet been observed.)

Orbital electron capture [process (3)] differs from the other modes of beta decay in the following respects:

- a. The electron wave functions correspond to bound atomic states, rather than to unbound particles in the continuum.
- b. The binding energy of an electron in a given shell or subshell is quantized and, therefore, the energy of the emitted neutrino is dis-

crete.

c. The orbital angular momentum of an electron in a given shell is unique.

The probability of finding an atomic electron bound in the i -th shell at the nuclear surface or inside the nucleus is proportional to the square of the atomic wave function evaluated at the nuclear surface. The chance that one of these bound atomic electrons will be captured by the nucleus while it is in the vicinity of the nucleus depends on the strength of the interaction between the electron and a bound proton (process 3). This interaction is known to be very weak; for example, an electron can traverse many meters of nuclear matter without interacting. This relatively long mean free path in nuclear matter is remarkable, in view of the density of nuclear matter, 1 or 2×10^5 tons/mm³. It is for this reason that beta processes are referred to as weak interactions.

The capture probability, P_i , of capture of an electron bound in the i -th shell, is proportional to

$$P_i \propto |\psi_i(0)|^2 \cdot W_i$$

where $\psi_i(0)$ is the atomic wave function of the i -th electron evaluated at the nucleus and W_i is the probability of capture of the electron by a proton in the nucleus due to a weak interaction (process 3). Values of $|\psi_i(0)|^2$ can be calculated using currently available atomic wave functions, as discussed below in more detail. However, in order to calculate W_i from theory, it is necessary to make assumptions about the exact nature

of the weak interaction (nuclear forces involved). (The weak interaction Hamiltonian in beta decay is formed by taking one or more of the five types of beta interaction: scalar, vector, axial vector, tensor, pseudoscalar.)

If one considers the ratio of capture probabilities from different atomic shells, K, L, M, two classes of orbital electron capture transitions can be distinguished: those in which W_i is the same for all shells (i.e., $W_M = W_L = W_K$) and those in which $W_M \neq W_L \neq W_K$. The former applies to allowed transitions ($\Delta J = 0, \pm 1, \text{no}$), whereas the latter case applies generally to forbidden beta transitions.

Thus, for allowed electron capture cases, the ratio of $P_M : P_L : P_K$ is proportional simply to the wave function density at the nucleus,

$|\psi_M(0)|^2 : |\psi_L(0)|^2 : |\psi_K(0)|^2$. Therefore, precise measurement of the capture ratios for allowed decays gives a sensitive experimental evaluation of these wave function probability ratios at the nucleus as a test of theoretically calculated values.

For forbidden transitions, for which $W_M \neq W_L \neq W_K$, a careful measurement of the capture ratios $P_M : P_L : P_K$, together with known wave functions (which are tested and in agreement with experiment for allowed transitions) permits the experimental determination of the ratios of the weak interaction probabilities, $W_M : W_L : W_K$, and thus gives information concerning the type and strength of the nuclear forces involved in weak interactions. (Specifically, experimental values of $W_M : W_L : W_K$, for forbidden-non-unique electron capture decays give all six nuclear matrix elements directly (1).)

Theoretical Considerations for Allowed Transitions

The first theoretical orbital electron capture calculations were done in 1942 by Marshak (2) for allowed L/K capture ratios. Segré (3) and Bouchez, Daudel, Daudel, and Mauxart (4) made similar calculations. Brysk and Rose (5) made extensive calculations for both allowed and forbidden L/K capture ratios, including capture from L_2 and L_3 subshells. Winter (6) repeated the Brysk and Rose calculations of allowed L_I/K capture ratios, but using Hartree-Fock wave functions (11), as discussed below.

Theoretical M/L-capture ratios for allowed and first-forbidden unique transitions have been calculated in the region $55 \leq Z \leq 90$ by Robinson (7) using M-shell wave functions of Brewer, Harmer, and Hay (8). Hubbard (1) made theoretical calculations of M/L capture for forbidden transitions. Wapstra and Van der Eijk (9) made M/L calculations with hydrogen-like wave functions using Slater screening. Bahcall (10) calculated M/L-capture ratios for allowed decays in the region $13 \leq Z \leq 37$, with and without electron exchange-atomic overlap, using the Hartree-Fock wave functions of Watson and Freeman (11).

The general theory of electron capture gives a capture probability, P_i , for capturing an electron bound in the i -th shell

$$P_i = K \left| \int \dots \right|^2 \cdot \left| \psi(r_i, Z) \right|^2 \cdot [W_0 + W_i]^2 n_i \quad (1)$$

where K is a universal constant, $\left| \psi(r_i, Z) \right|$ is the wave function of an electron in the i -th shell, n_i is the number of electrons in the i -th

shell, W_0 is the total energy available for the electron capture transition in units of $m_0 c^2$ (511 keV), and W_i is the total binding energy in $m_0 c^2$ units of the i -th electron with rest mass included.

The nuclear matrix elements $|\int \dots|$, which are related to the weak interaction probability W_i , discussed above, may be written in schematic form:

$$|\int \dots| = \int_{\tau} \psi_f^* H \psi_i d\tau$$

where ψ_f^* and ψ_i are the nuclear wave functions for the final and initial states of the nucleus, and H is an appropriate operator describing the interaction. Physically, the square of the matrix elements, $|\int \dots|^2$, should be understood as the extent of overlap between the final and initial states of the nucleus, and hence gives the weak interaction probability.

In order to use equation (1), one must have some knowledge of the nuclear matrix elements, which are poorly known, since they depend on specifically nuclear properties. However, the matrix elements cancel out when ratios of allowed electron capture from different shells, EC/β^+ ratios, β^-/β^+ ratios, or an allowed beta spectral shape are taken. Thus, in the specific case of L/K capture ratios for allowed transitions, one obtains

$$(P_L/P_K)^0 = \left(\frac{q_L}{q_K}\right)^2 \left(\frac{g_L}{g_K}\right)^2 \left(\frac{n_L}{n_K}\right) \quad (2)$$

and for allowed M/L capture ratios, one has

$$(P_M/P_L)^0 = \left(\frac{q_M}{q_L} \right)^2 \left(\frac{g_M}{g_L} \right)^2 \left(\frac{n_M}{n_L} \right) \quad (3)$$

where $q_L = W_0 + W_L$, $q_M = W_0 + W_M$, $q_K = W_0 + W_K$, the energy of the neutrino emitted from each shell; g_K , g_L , and g_M are the atomic wave functions for electrons in the K, L, M shells, respectively, evaluated at the nuclear surface; i.e., $g_K^2 = |\psi_K(0)|^2$, etc.; n_K , n_L , and n_M are the respective numbers of electrons in the K, L, and M shells. (For L_1/K capture, $n_{L_1}/n_K = 1$)

To make use of equations (2) and (3), one needs values of the wave function ratios g_L/g_K and g_M/g_L . The most extensive work on g_L/g_K ratios is that of Brysk and Rose (5), who evaluated wave functions for K, L_1 , L_2 , and L_3 subshells, using a Thomas-Fermi-Dirac atom with corrections for screening, finite nuclear size, relativistic effects, and variation of the wave functions over the nuclear volume.

A number of precision measurements of allowed L/K capture ratios have been reported in the last decade. These have been reviewed by Robinson and Fink (12), who pointed out that a significant discrepancy of up to 25 percent exists between experiment and theory as represented by equation (2). Bouchez and Depommier (13) also reviewed the experimental results. For Ar^{37} , the discrepancy amounted to about 25 percent (12).

This discrepancy led Bahcall (14) to reexamine the theory. He introduced previously neglected correction terms, arising from exchange and atomic overlap among the electrons of the initial and final states of the

transforming nucleus. Earlier, Odier and Daudel (15) had suggested that a correction for electron correlations was required.

Bahcall's calculations (14) are limited to the region $13 \leq Z \leq 37$, where analytic Hartree-Fock wave functions are available from the work of Watson and Freeman (11). The Bahcall exchange corrections arise from the fact that L_I capture can occur in three experimentally indistinguishable ways:

1. capture of a 2s electron with the 1s and 3s electrons appearing in the final 1s' and 3s' states;
2. capture of a 1s electron with a 2s electron appearing in the final 1s' shell;
3. capture of a 3s electron with a 2s electron appearing in the final 3s' shell.

Process 1 is the only one taken into account by the usual theory (equation 2).

For capture from the M_I subshell, there are also three experimentally indistinguishable processes, only the first process being considered by the usual theory (equation 3):

1. capture of a 3s electron with the 1s and 2s electrons appearing in the final 1s' and 2s' states;
2. capture of a 1s electron with a 3s electron appearing in the final 1s' shell;
3. capture of a 2s electron with a 3s electron appearing in the final 2s' shell.

The theoretical L/K capture ratio, including corrections for a

small amount of L_2 capture and exchange-overlap, is given by

$$\begin{aligned} (P_L/P_K)_{\text{Theory}} &= \left(\frac{q_L}{q_K}\right)^2 \left[\left(\frac{g_{L_1}}{g_K}\right)^2 \left\{ 1 + \left(\frac{g_{L_2}}{g_{L_1}}\right)^2 \right\} \right] \cdot X^{L/K} \quad (4) \\ &= (P_L/P_K)^0 \cdot X^{L/K} \end{aligned}$$

where $X^{L/K}$ is the Bahcall exchange correction factor for effect of exchange on the L_1/K capture ratio, given by

$$X^{L/K} = \left| \frac{\langle 1s' | 1s \rangle}{\langle 2s' | 2s \rangle} \right|^2 \left[\frac{1 - \frac{\langle 1s' | 2s \rangle \psi_{1s}(0)}{\langle 1s' | 1s \rangle \psi_{2s}(0)} - \frac{\langle 3s' | 2s \rangle \psi_{3s}(0)}{\langle 3s' | 3s \rangle \psi_{2s}(0)}}{1 - \frac{\langle 2s' | 1s \rangle \psi_{2s}(0)}{\langle 2s' | 2s \rangle \psi_{1s}(0)} - \frac{\langle 3s' | 1s \rangle \psi_{3s}(0)}{\langle 3s' | 2s \rangle \psi_{2s}(0)}} \right]^2 \quad (5)$$

where $\langle ms' | ns \rangle$ is the overlap between the ms' electron in the final atomic state and the ns electron in its initial state, where m and n are integers of 1, 2, 3, etc. The result can be expressed in the form given by Bahcall (14), based on Watson-Freeman wave functions (11).

$$X^{L/K} = 1 + \frac{2.810}{Z} + \frac{13.76}{Z^2} + \frac{75.2}{Z^3} \quad (6)$$

(The ratio of L_2/L_1 capture of M_2/M_1 capture is approximately

$$\left| \frac{\psi_{p_{1/2}}(0)}{\psi_{s_{1/2}}(0)} \right|^2 \approx \frac{3}{16} (\alpha Z)^2$$

for $Z < 40$, where $\alpha = 1/137$, the fine-structure constant, assuming a point nucleus.)

Similarly, for M/L capture, the theoretical ratio is given by

$$\left(\frac{P_M}{P_L}\right)_{\text{Theory}} = \left(\frac{q_M}{q_L}\right)^2 \left(\frac{\xi_{M_1}}{\xi_L}\right)^2 \left[X^{M/L} + \left(\frac{\xi_{M_2}}{\xi_{M_1}}\right)^2 - \left(\frac{\xi_{L_2}}{\xi_{L_1}}\right)^2 \right] \quad (7)$$

where, as above,

$$\left(\frac{\xi_{M_2}}{\xi_{M_1}}\right)^2 \cong \left(\frac{\xi_{L_2}}{\xi_{L_1}}\right)^2$$

Hence,

$$\left(\frac{P_M}{P_L}\right)_{\text{Theory}} = \left(\frac{P_M}{P_L}\right)^{\circ} \cdot X^{M/L} \quad (7a)$$

where in a similar way, based on the Watson-Freeman wave functions (11),

$$X^{M/L} = 1 + \frac{5.593}{Z} - \frac{59.5}{Z^2} + \frac{1111}{Z^3}$$

from Bahcall (10).

Theoretical calculations of $\left(\frac{P_M}{P_L}\right)$ with exchange and without exchange in the region of $13 \leq Z \leq 37$ have been given by Bahcall (10). In the region $55 \leq Z \leq 90$, theoretical values of $\left(\frac{P_M}{P_L}\right)^{\circ}$ without exchange have been computed by Robinson (7).

Comparison of Theory and Previous Experimental Results

The most recent comparison of precision L/K capture ratios for allowed and first-forbidden transitions has been given by Fink (16). Similarly, a comparison of M/L capture experiments with theory (equations 3 and 7) has been given by Fink and Ledingham (17). Figure 1, taken from reference 17 shows the following features which show how experimental M/L capture ratios compare with theory.

Inset [shows] the region near $Z = 18$ with the previous result for Ar^{37} . . . [19].

Curve A-A is the theoretical estimate of Wapstra, et al., . . . [9] based on hydrogen-like wave functions with Slater screening. No correction for electron exchange-atomic overlap is included.

Curve B-B in the region $Z = 13$ to $Z = 37$ is the theoretical result of Bahcall, . . . [10], based on Hartree-Fock wave functions calculated by Watson and Freeman, and in the region $Z = 55$ to $Z = 90$ is the theoretical result of Robinson, . . . [7], based on M-shell wave functions of Brewer, Harmer, and Hay [8]. The region $Z = 37$ to $Z = 55$ is a smooth interpolation between the results of Bahcall [10] and those of Robinson [7]. No correction for electron exchange-atomic overlap is included.

Curve C-C is the same as B-B, except that the electron exchange-atomic overlap correction calculated by Bahcall, . . . [10], has been applied between $Z = 13$ and 37. This correction has been extrapolated in the region of $Z \geq 37$.

Δ indicates points from direct experimental measurements of the M/L capture ratio with gaseous internal sources in single- or multi-wire proportional counters.

\bigcirc indicates all other values of M/L-capture ratios derived from precision measurements of $(L + M + N + \dots)/K$ ratios, with values of the L/K capture ratio taken either from a precision experimental measurement or from exchange-corrected theory in cases where an accurate value of Q_{EC} is known from independent measurements.

The experimental points are as follows:

- a) Ar^{37} , $M/L =$ [see results of present investigation]
($Q_{EC} = 815 \pm 5$ keV)
- b) Ge^{71} , $M/L = 0.16 \pm 0.08$ ($Q_{EC} = 237 \pm 5$ keV) . . . [38]

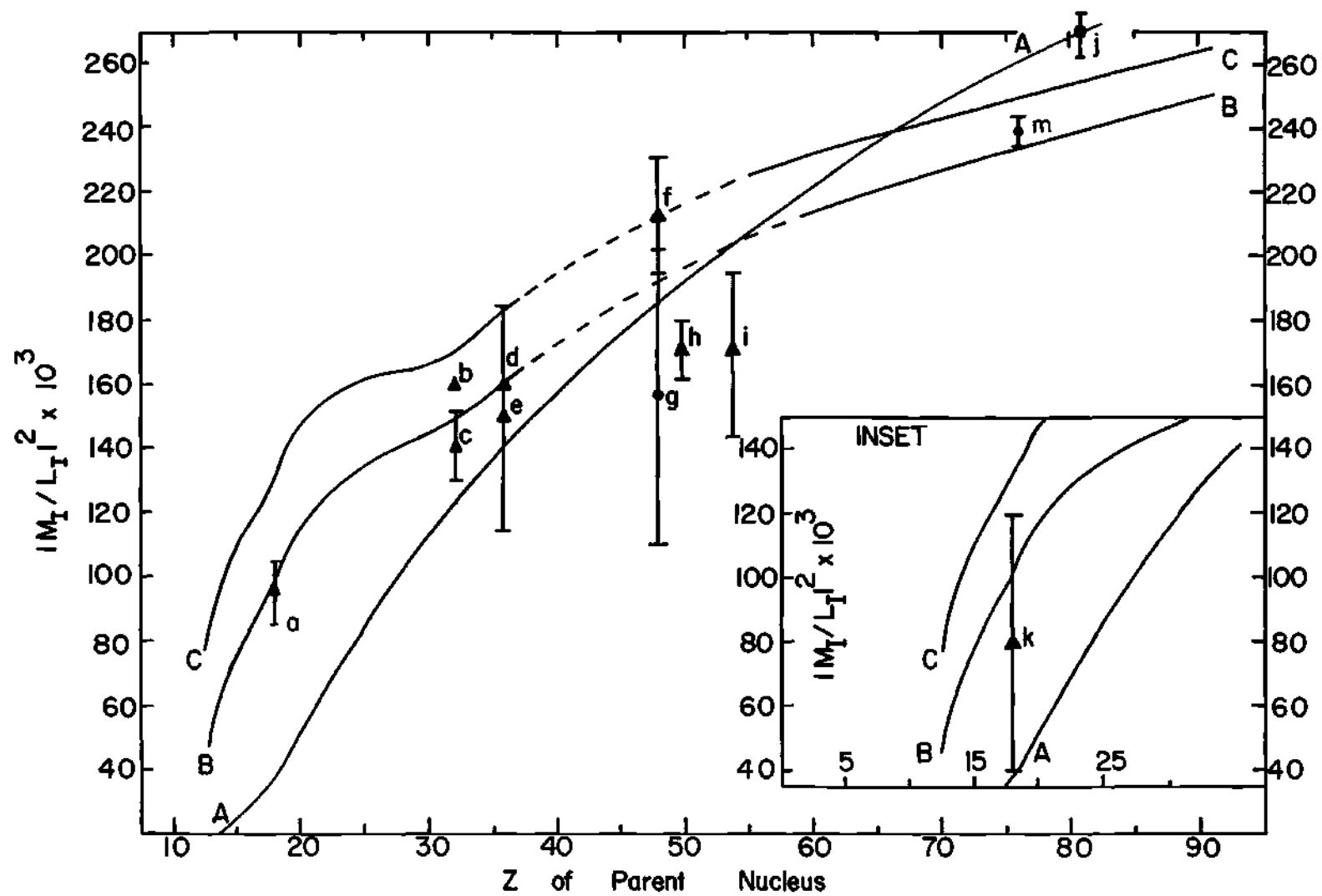


Figure 1. Comparison of Experimental M/L Orbital Electron Capture Ratios with Theoretical Results

- c) Ge^{71} , $M/L = 0.141 \pm 0.010$ ($Q_{\text{EC}} = 231 \pm 3$ keV) . . . [34]
 d) Kr^{79} , $M/L = 0.16 \pm 0.08$. . . [38]
 e) Kr^{79} , $M/L = 0.150 \pm 0.035$. . . [39]
 f) Cd^{109} , $M/L = 0.232 \pm 0.020$. . . [40]

Note: Since $Q_{\text{EC}} = 80^{+7}_{-3}$ keV to the 88 keV, 40 sec $\text{Ag}^{109\text{m}}$ state,

$$q = (80 - 0.775)^2 / (80 - 4.02)^2 = 1.087, \text{ whence}$$

$$|M_{\text{I}}/L_{\text{I}}|^2 = \frac{0.232 \pm 0.020}{1.087} = 0.213 \pm 0.018, \text{ which is plotted.}$$

- g) Cd^{109} , $(M + N)/L = 0.170 \pm 0.005$, from experiments with NaI(Tl) crystals containing Cd^{109} [41], and using $q = 1.087$, a value of $|M_{\text{I}}/L_{\text{I}}|^2 = 0.156 \pm 0.05$ is plotted.

- h) Sn^{113} , $M/L = 0.20 \pm 0.01$. . . [42].

Since $Q_{\text{EC}} = 49 \pm 3$ keV to the 393 keV level,

$$q = (49 - 0.868)^2 / (49 - 4.445)^2 = 1.167, \text{ from which}$$

$$|M_{\text{I}}/L_{\text{I}}|^2 = \frac{0.20 \pm 0.01}{1.167} = 0.171_4 \pm 0.01 \text{ is plotted.}$$

- i) $\text{Xe}^{127\text{g}}$, $M/L = 0.183 \pm 0.025$. . . [43]

- j) $\text{Tl}^{202\text{g}}$, $M/L = 0.269 \pm 0.007$, to the 440 keV level in Hg^{202} , from crystals of NaI(Tl) containing $\text{Tl}^{202\text{g}}$ [47] $Q_{\text{EC}} = 797$ keV to the 440 keV level. This transition is first-forbidden unique and, in a strict sense, it cannot be compared rigorously with theory for allowed transitions. However, the difference may be smaller than the experimental and theoretical errors. For this reason, the location of the point for $\text{Tl}^{202\text{g}}$ is interesting.

Os^{185} , $M/L = 0.254 \pm 0.005$, to the 646 keV level in Re^{185} , from crystals of NaI(Tl) containing Os^{185} (45). This is a first-forbidden transition. $Q_{\text{EC}} = 336$ keV to 646 keV level of Re^{185} .

Since $Q_{\text{EC}} = 336$ keV

$$q = (336 - 2.93)^2 / (336 - 12.52)^2 = 1.0602$$

$$|M_{\text{I}}/L_{\text{I}}|^2 = \frac{0.254 \pm 0.005}{1.0602} = 0.239 \pm 0.005$$

In the case of L/K capture ratios, the Bahcall correction for exchange (equation 6) applied to the theoretical results for allowed transitions of Brysk and Rose (5) appears to bring theory into agreement with experimental values within the error limits of the latter. For example,

For example, the Bahcall exchange correction of 22 percent in the case of Ar^{37} decay brings the L/K capture ratio calculated from Brysk and Rose into excellent agreement with experiment ($P_L/P_K = 0.102 \pm 0.003$)(16).

However, Winter (6) pointed out that the procedure of adjusting the results of Brysk and Rose (5) (who used hydrogen-like wave functions with screening based on internal conversion coefficient calculations) with the Bahcall exchange correction (which makes use of the very accurate analytic Hartree-Fock wave functions of Watson and Freeman (11)) is logically inconsistent, in spite of the fact that it leads to good agreement for allowed L/K capture ratios. Therefore, Winter (6) recalculated theoretical L/K capture ratios with exchange, using the same Hartree-Fock wave functions (11) as used by Bahcall (10) for the exchange correction. When these calculations are compared with experiment (16), the experimental values are found to lie somewhat lower than the theoretical predictions of Winter corrected for Bahcall exchange. For allowed M/L capture ratios, the discrepancy between experiment and theoretical values with exchange (10) is considerably larger, using the Hartree-Fock wave functions of Watson and Freeman (11) only.

This discrepancy for both L/K- and M/L-capture ratios may arise from assumptions involving the Hartree-Fock wave functions (11), especially the screening assumptions to which the M-shell is more sensitive than the L-shell.

Since the appearance of Bahcall's calculations (10,14), based on Watson-Freeman (11) wave functions, several new calculations of accurate analytical SCF Hartree-Fock wave functions for the low-Z region have been reported (23,24,25). It remains to be seen whether these newer wave

functions will bring theoretical L/K- and M/L-orbital capture ratios into closer agreement with experiment.

Figure 1 shows a complete lack of information on M/L capture ratios for $Z < 32$ (Ge^{71}). Also, the theoretical curves differ from one another most in the low-Z region. Therefore, the most sensitive test of M/L capture theory would be for a low-Z nuclide.

Choice of a Low-Z Nuclide: Ar^{37}

An ideal low-Z case is that of 35.1 day Ar^{37} decay ($Z = 18$), for which the predicted exchange correction, $X^{M/L}$, amounts to + 31.6 percent (10). The electron-capture decay of Ar^{37} is allowed ($\log ft = 5.1$) and proceeds entirely to the ground state of Cl^{37} . The transition energy is 813.8 ± 0.7 keV (18). The inset in Figure 1 shows the only previous experimental result for the Ar^{37} M/L capture ratio (19). The error limits on this result are too large to determine which theory agrees best with experiment. These large error limits in the previous result (19) arose chiefly from an inability to separate unambiguously the M- and L-spectra, due to uncertainties in spectral shapes produced in proportional counters by events having energies below about 300 eV.

Recent investigations (20, 21, 22) of the pulse height distributions from proportional counters due to single- and multiple-electron events and improvements in electronic technique have made it possible to repeat the Ar^{37} M/L capture measurement with much greater accuracy.

The K-, L-, and M-Spectrum in Ar^{37} Decay

The electron binding energies in the daughter chlorine ($Z = 17$) atom are 2822.4 ± 0.3 , 270.2 ± 0.4 , 201.6 ± 0.3 , 200.0 ± 0.3 , 17.5 ± 0.4 ,

and 6.8 ± 0.4 eV for the K, L_1 , L_2 , L_3 , M_1 , and $M_{2,3}$ shells, respectively (32). Following orbital electron capture by the nucleus, the daughter atom is left with a vacancy in one of its inner atomic shells. The subsequent atomic rearrangement of these inner shell vacancies (33) causes emission of x-rays and/or Auger electrons of energies corresponding closely to binding energy differences of the daughter atom.

In particular, after K-electron capture, an electron from a higher shell falls into the K-shell vacancy, from which appears either a K_α x-ray (from K- $L_{2,3}$ transitions), a K_β x-ray (from K-M transitions), or Auger electrons (from a radiationless transition). In any case, vacancies transferred to the L- or M-shells are in turn filled by electrons from higher shells, etc., so that, if there is no escape of energy from the sensitive volume of the counter, the K-capture event will display the full K-shell binding energy of the daughter atom. Similar considerations apply to L-electron capture, in which case the resolution of proportional counters in the L energy region of chlorine is insufficient to resolve the L_1 , L_2 , and L_3 subshells.

Since the energy released in Ar^{37} M-electron capture lies below about 17.5 eV, the event releases a single electron of energy insufficient to produce an ion pair. Therefore, M-capture in Ar^{37} decay gives rise to a single-electron spectrum similar to that obtained with ultraviolet photons (see Chapter II, page 28).

The relative frequency of electron capture from the K-, L-, and M-shells in Ar^{37} is approximately 100:10:1, so that long counting times are necessary for the M spectrum in order to obtain data which are statistically as good as for the L spectrum.

CHAPTER II

EXPERIMENTAL MEASUREMENTS

Preparation and Handling of Radioactive Ar³⁷ Source

The Ar³⁷ source was prepared by an irradiation of natural argon in the Georgia Tech reactor. The source was contained under pressure in a vessel filled with Na-Pb alloy* to assure long-term freedom from possible atmospheric contamination. From the spectra obtained, it was evident that radioactive contamination by Ar³⁹, Ar⁴¹, or other activities was negligible, as discussed below.

Description of Single-wire Proportional Counter

A small single-wire aluminum proportional counter (see Figure 2), having a sensitive length of 20 cm and an inner diameter of 4.17 cm, was used. This was fitted with earthed guard tubes and with field tubes. An external window of 0.65 cm diameter was provided which could be used either with Mylar (40 mg/cm²) or with a 23.5 mg/cm² beryllium window to admit external ultraviolet or x-rays for calibration. The center wire was of stainless steel of 0.0075 cm diameter. The counter was operated with negative high voltages on the case and field tubes and was shielded by 5 cm of lead. The use of negative high voltage (of the order of 2000 volts for one atmosphere pressure) on the outer case of the counter is superior to grounding of the case and positive high voltage on the center wire, be-

* Donated by Ethyl Corporation, Baton Rouge, Louisiana.

cause a coupling capacitor between the center wire and first stage of the preamplifier is then unnecessary. Normally, the coupling capacitor must withstand several thousand volts with no leakage, corona discharge, or other spurious discharges which give pulses similar to the signal pulses, and it must have good response to relatively fast rising pulses over a fairly large dynamic range.

The negative high voltage was applied to the counter cathode from a Fluke HV power supply (regulated to 0.05 percent). An RC filter ($R \approx 10$ megohm, $C \approx 1$ microfarad) was interposed for smoothing the ripple due to charge collection in the counter. This is shown in the block diagram, Figure 3.

Another Fluke power supply was used to supply negative high voltage to the field tubes, also with RC smoothing.

The voltage applied to the field tubes was calculated from the dimensions of the counter to be about 60 percent of the outer case voltage; however, experimentally, optimum resolution for the 2.82 keV K-peak in Ar^{37} decay was obtained with a field tube voltage of 72 percent of the outer case voltage.

With proportional counters, one can obtain output pulses proportional to the primary ionization produced by an x-ray or an electron in the sensitive volume of the counter. The primary ionization produced in the counter is then subject to gas amplification, so that it is important, in order to have a linear response, that the gas amplification factor be independent of the primary ionization, i.e., the amplification gain is the same for ionization produced by particles of different energies and independent of the location of the primary ionization event. This implies

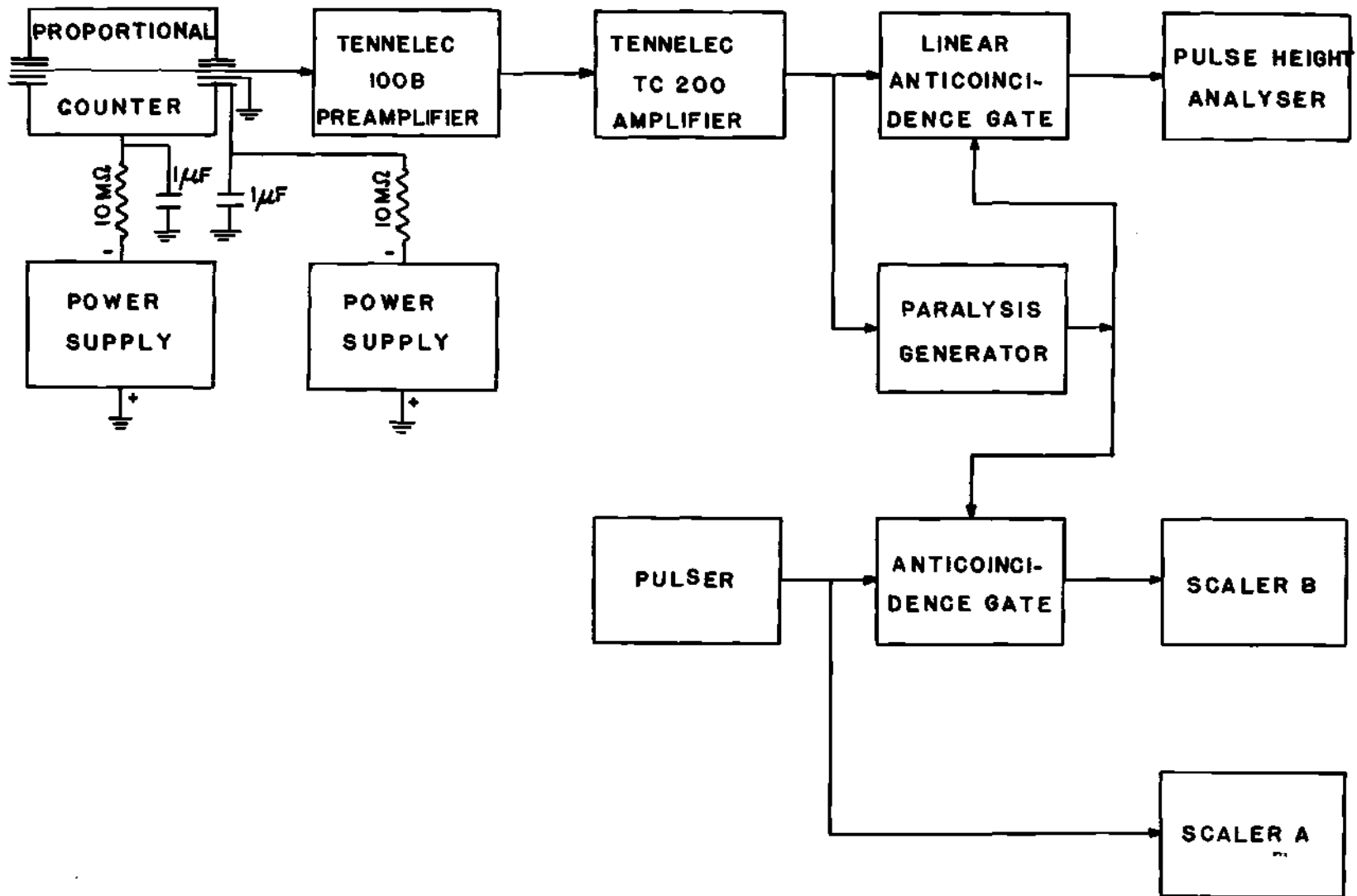


Figure 3. Block Diagram of Electronic Detection System

that the field distribution must be the same in the entire volume in which primary ionization occurs. Any distortion of the field can lead to changes in the gas amplification. This requires, therefore, that the central wire be uniformly circular in cross section and have a constant diameter. The surface must also be free of inhomogeneities and defects. The wire must be precisely centered in the cathode cylinder.

The influence of the centering of the anode wire inside the field tubes is critical for good resolution and peak-to-valley ratio in the L- and M-region of the Ar³⁷ electron capture decay. All these requirements were taken into account in designing the counter.

Gas Filling

The gas filling consisted of argon with 15 percent propane admixed, after evacuation of the counter to better than 10^{-5} Torr for several days. No differences were observed with ordinary high-purity tank argon and ultra-high purity argon having less than 10 ppm total impurities with actual gas analysis supplied by the manufacturer. Mixtures of argon-methane and argon-acetylene also were investigated, but the best resolution was obtained with an argon-propane mixture. Runs were made at pressures up to two atmospheres. Great care was taken to keep the counter and associated vacuum system free of oxygen and water vapor, which, if present, form negative ions by electron attachment.

Electron attachment manifests itself by a loss in resolution (tail-ing on the low-energy side of a peak), a decrease in proportionality, a reduction in gas gain, and the appearance of an appreciable number of small afterpulses. (See discussion concerning afterpulses beginning on

page 27.)

Electronic System

The block diagram of the electronic detection system is shown in Figure 3. The center wire of the counter was DC-connected to the grid of the first tube (Amperex 6922) of a Tennelec 100B preamplifier, the output of which was fed into a Tennelec TC-200 amplifier, which was operated in a doubly-differentiated mode with time constants typically of the order of 1.6 microseconds. These pulses were fed via a linear anticoincidence gate into a Nuclear Data 128-channel analyzer. The gating pulse was triggered at the zero cross-over point of the pulse to be analyzed. The gate was controlled by pulses generated by a paralysis pulse generator. A transistorized paralysis generator was constructed (26) to eliminate the possibility of small afterpulses which follow large pulses (see discussion of afterpulses below). A block diagram of the paralysis pulse generator is shown in Figure 4, and its circuit diagram is given in Figure 5.

The paralysis pulse generator was constructed to have zero-time recovery, and it produced gating pulses of width variable from zero to 50 milliseconds. The zero time recovery feature means that a pulse, due to cosmic rays, K, L, or M events, which arrives at a time during which the modified linear anticoincidence gate (Sturup Model 1450) is closed by a paralysis pulse, triggers an additional paralysis pulse which continues to keep the gate closed in order to prevent detection of possible afterpulses. The triggering level of the paralysis pulse generator was set high enough to avoid any danger of triggering paralysis pulses by noise. The sequence of pulses through the paralysis pulse generator and linear

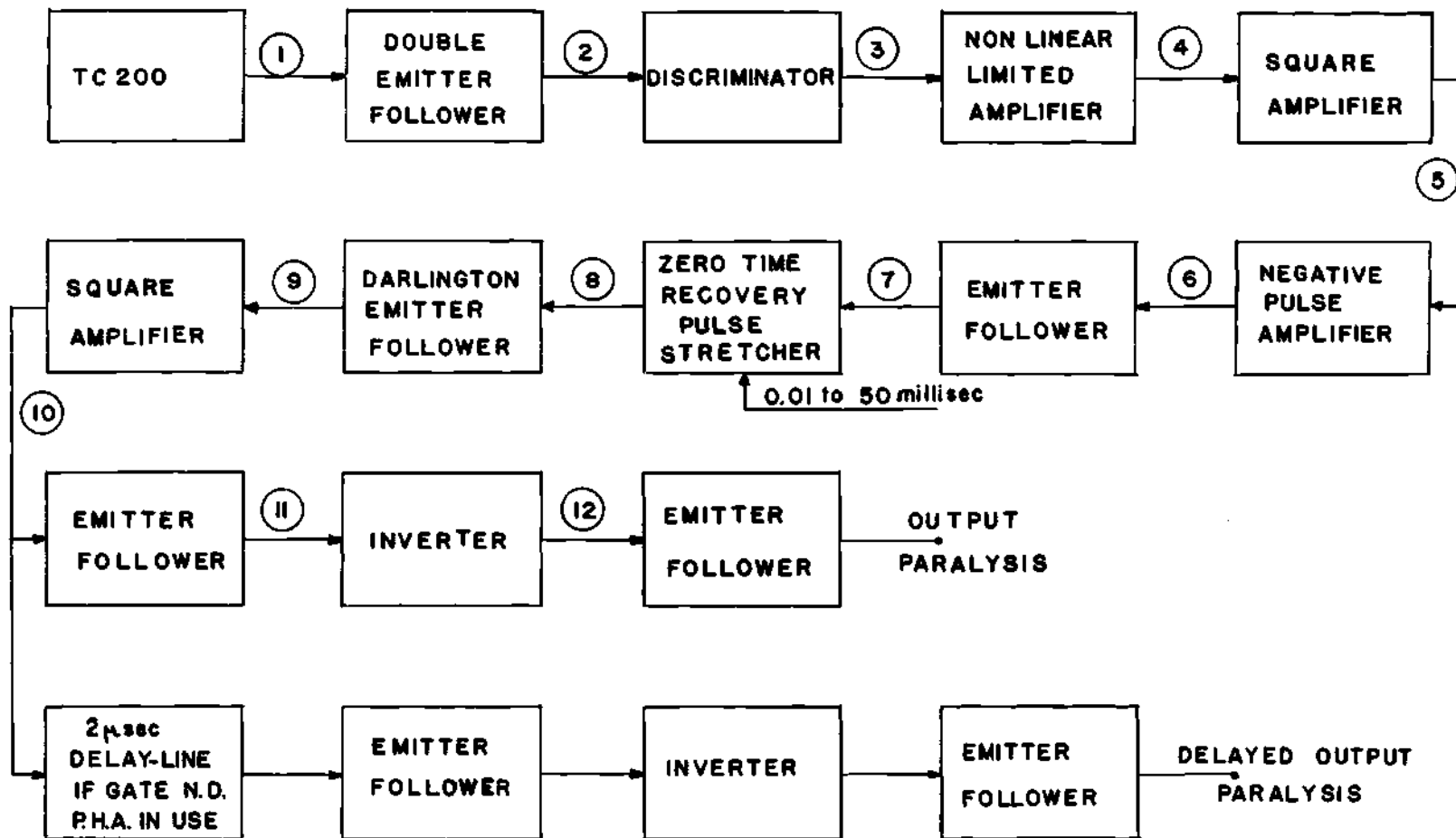


Figure 4. Block Diagram of Paralysis Pulse Generator

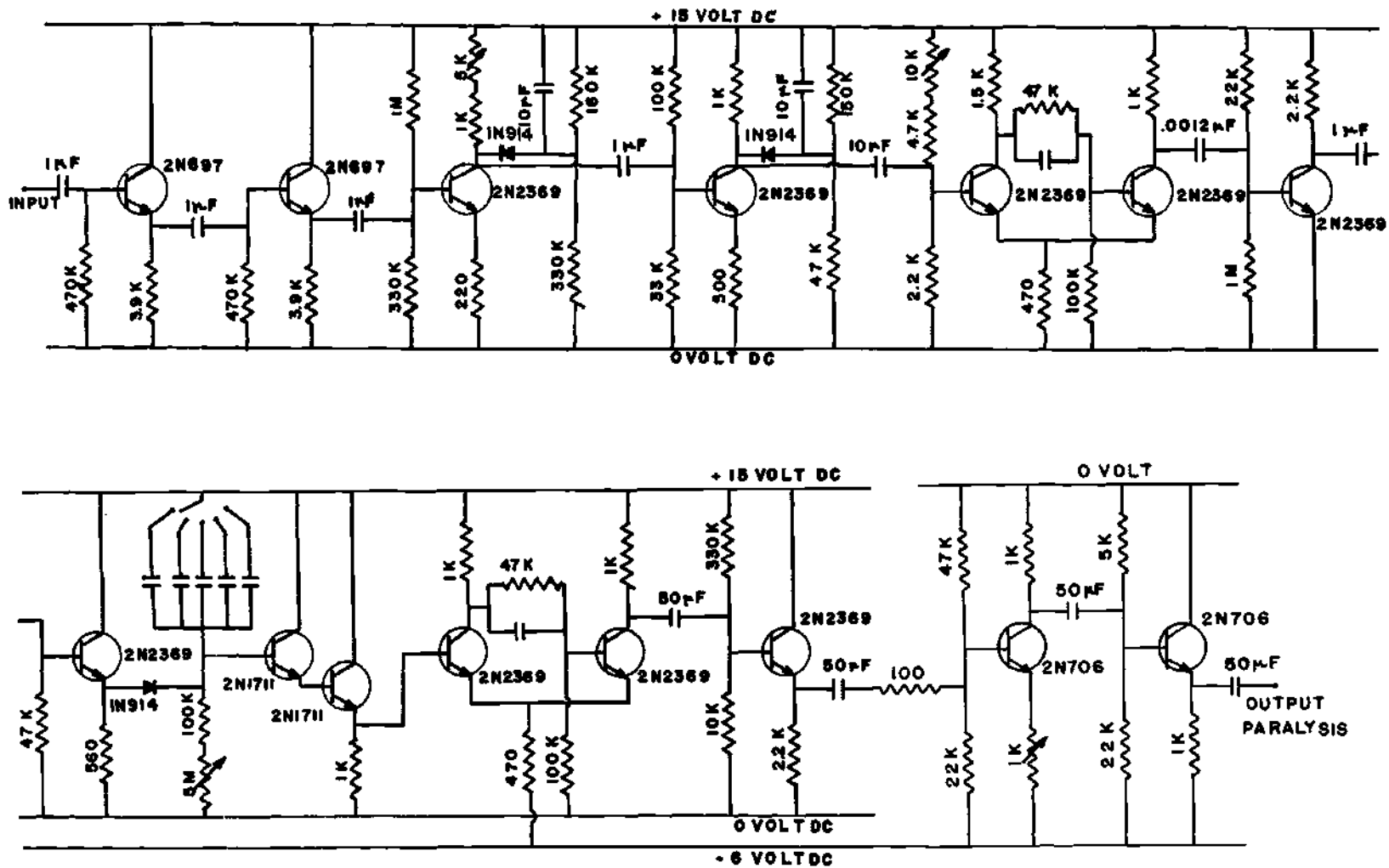


Figure 5. Circuit Diagram of Paralysis Pulse Generator

anticoincidence gate is shown in Figure 6, where the numbers in circles on the left indicate the corresponding test points in Figure 4.

A modification of the linear anticoincidence gate (Sturupp Model 1450) was necessary, because the gate driver of the gate did not have zero time recovery. The paralysis gating pulse from the paralysis pulse generator was fed to a suitable point in the gate driver circuit of the gate. By this means, zero time recovery was accomplished in the linear anticoincidence gate. This modification, together with other circuit changes in the Sturupp Model 1450 linear anticoincidence gate, is shown in Figure 7.

To measure the effective open time of the linear anticoincidence gate, a second anticoincidence gate, also modified to have zero time recovery (Figure 7), was operated in parallel with the first one. The paralysis pulse triggered both gates simultaneously. The signal input of the second gate was fed by a pulser. Scaler A, connected to the pulser, and scaler B (Figure 3), connected to the output of the second gate, determined the ratio of open/total time.

The gain stability of the experimental system as determined by the channel shift of a calibration peak typically was less than one percent in 24 hours. The resolution stability of the Ar^{37} K-peak (2822 eV) was investigated as a function of time after filling the counter. The resolution (full-width at half-maximum) typically was 21 ± 1 percent at gross count rates of 4000 counts/minute and was constant over a period of at least 70 hours after filling.

At counting rates above 300 counts/second, small pulses can be created by the clipping of large pulses by the electronic system or by

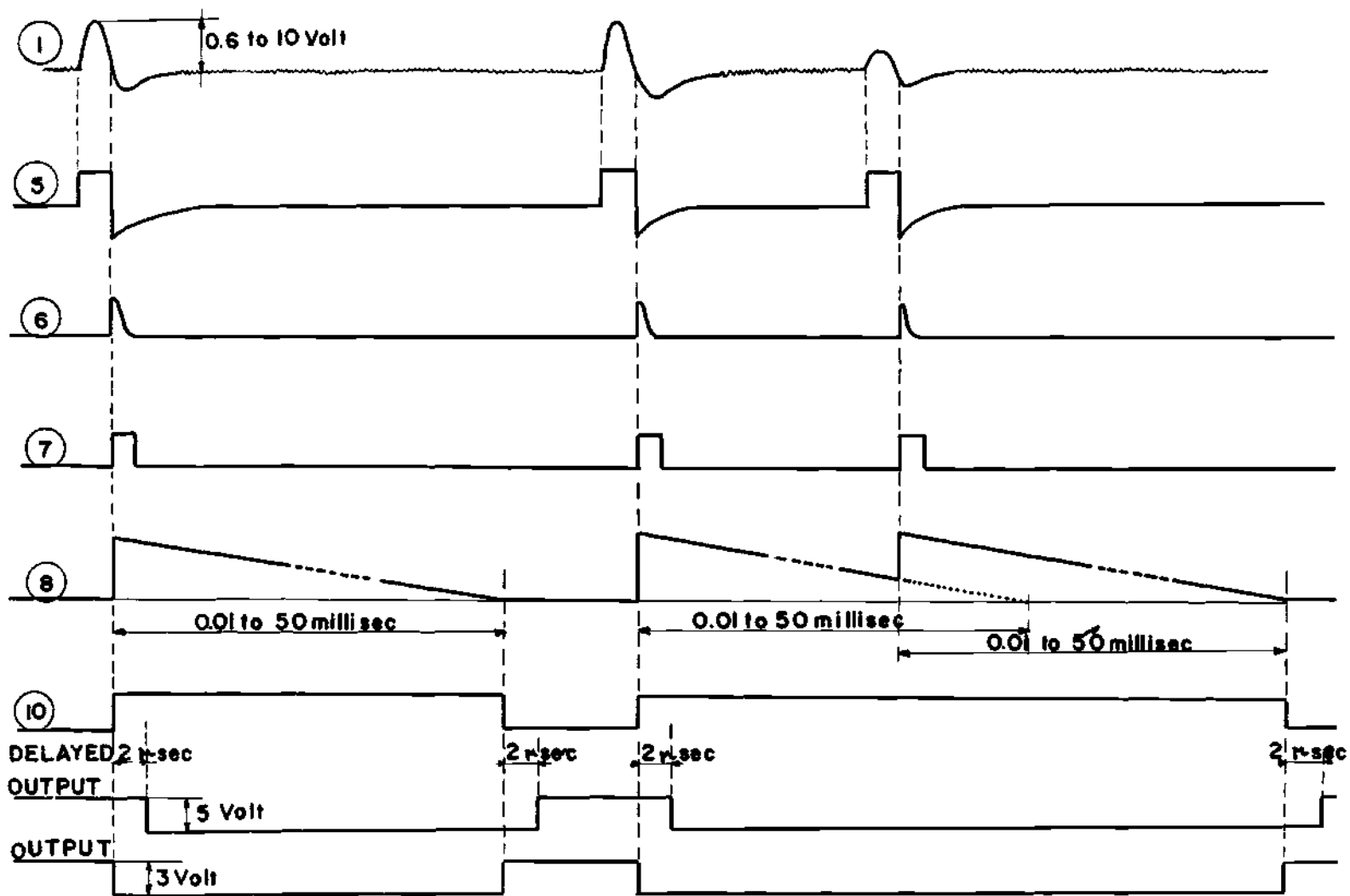


Figure 6. Pulse Sequence Diagram of Paralysis Pulse Generator

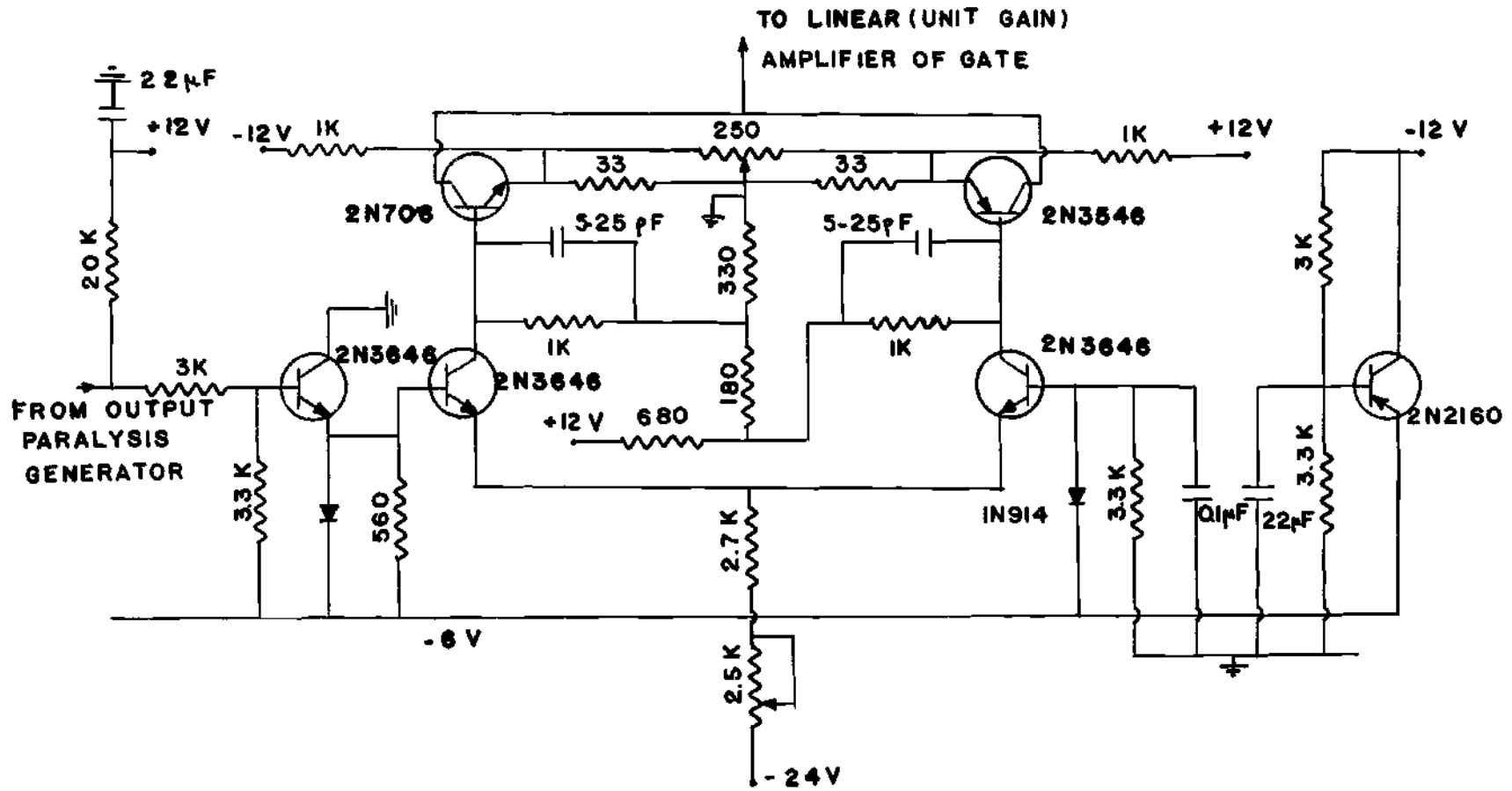


Figure 7. Modification of Linear Anticoincidence Gate to Produce Zero Time Recovery

non-zero time recovery of the baselines in the Tennelec 100B - TC-200 amplifier system. Radiative electrical pickup or line transients also can induce small pulses in the system. In the present investigation, total counting rates were limited to 100 counts/second, in order to minimize any clipping effect, and electrical pickup was minimized by careful electrostatic screening and grounding. Line power was provided by a private regulated, filtered 115 volt, 60 cycle system.

Afterpulses in Proportional Counters

When the paralysis pulse generator was disconnected, small afterpulses in the Ar³⁷ experiments were observed in the energy region below about 100 eV. Most of these afterpulses had time delays of less than about 700 microseconds. These afterpulses have been reported previously in Ar³⁷ and Cl³⁶ studies (19,27) in proportional counters. Afterpulses up to 400 microsecond delays also have been found in Geiger-Müller counters (28).

The origin of afterpulses is not understood at present. Two possible mechanisms giving rise to afterpulses have been suggested. The first of these is electron attachment leading to negative ion formation, following the primary ionizing event. Owing to the fact that negative ions are born anywhere in the sensitive volume of the counter, they will exhibit a variety of transit times for collection on the anode center wire, depending on the size of the counter and on the molecular weight and charge of the negative ion. If this mechanism is present, the afterpulses will depend on the concentration of oxygen, moisture, or other electronegative impurities present (or introduced for investigative pur-

poses) in the gas. A second mechanism can be termed the "positive ion echo effect." Since most of the positive ions are born in the electron avalanche which occurs within a few wire diameters of the center wire, they travel as a bunch towards the cylindrical cathode walls, and their transit time for charge collection is relatively constant. When the positive ion bunch arrives at the cathode walls, it very likely causes emission of a secondary electron bunch, which then travels back to the center wire with essentially constant transit time, where it initiates another avalanche with formation of another positive ion bunch, which repeats the process. This "echo effect" is repeated with decreasing intensity at constant time intervals.

These two mechanisms for formation of afterpulses lead to two very different time distributions of afterpulses, following a primary ionization event. Therefore, an investigation of the time distribution of afterpulses in proportional counters may enable us to distinguish the process chiefly responsible.*

Single-electron Spectroscopy

When the energy of a capture event is lower than that required to produce an ion pair (* 27 eV), the primary single electron triggers an avalanche whose pulse height distribution in the proportional region has been carefully investigated (20, 21, 22, 29) and found to be dependent on experimental conditions, such as gas gain, type of counting gas, and pressure. Contrary to earlier thinking (30), the single-electron spectrum

* This time distribution experiment is in progress (March, 1967) by D. S. Harmer, H. Genz, and R. W. Fink, using a two-parameter analyzer, for energy and time analysis.

cannot be represented by an exponential function (e^{-x}), nor by a quasi-exponential ($x^1 e^{-x}$) function (29). Therefore, as shown by references 20, 21, and 22, in order to know the exact single-electron spectrum for a given experimental system, it is necessary to determine the single-electron spectrum experimentally.

The counter was operated at gas gains up to 10^4 , well within the range of proportionality (31).^{*} With this gas gain, the mean pulse height of single electrons was approximately ten times greater than noise.

Single electrons were generated in the counter by introducing ultraviolet photons from an incandescent UV bulb through the 40 mg/cm^2 Mylar window, producing photoelectrons from the aluminum walls. These photoelectrons have maximum energies of only a few eV.

In the Ar^{37} experiments, the spectral shape of single electrons was determined for each Ar^{37} M-capture spectral measurement (see below).

Energy Calibrations, Optimization for the Ar^{37} Spectrum,
and System Stability

In order to get good linear response from a proportional counter, the quantity mE should be kept below a value of 10^8 , where m is the gas gain and E is the energy of the primary ionizing event in eV (31). An external source of 2.9-year Fe^{55} , was used as a calibration standard (K_{α} x-rays = 5.9 keV). If the gas gain is set at about $m = 10^4$, then the quantity mE is 2.8×10^7 for the Ar^{37} K-peak and is 5.9×10^7 for the K_{α}

^{*}The charge sensitivity of the Tennelec 100B preamplifier is known within 10 percent to be 10^{-14} Coulomb per 10 millivolts applied to the input grid, which corresponds to 6×10^4 electrons deposited on the center anode wire.

peak of Fe^{55} . Thus, in order to keep mE for the Fe^{55} standard within the limits, the gas gain was kept below 10^4 . The resolution of the Fe^{55} x-rays was typically 16 ± 1 percent (FWHM).

The Ar^{37} K peak at 2822 eV was observed periodically throughout the runs to check counter resolution at this energy (21 ± 1 percent FWHM), to check gain stability (which was typically one-half channel per 24 hours), and for the purpose of determining the L/K intensity ratio, a quantity required in the evaluation of the corrections discussed below.

Since the gas gain of cylindrical proportional counters, m , is proportional to e^{aV} , where a is a constant and V is the applied voltage, a small variation in the counter high voltage leads to an exponential variation in the gas gain. In the present experiment, a variation of one volt in the Fluke high voltage power supply at 2000 volts (0.05 percent) at one atmosphere counter gas pressure gave a shift of one-half channel in the 128-channel analyzer. This represents the limit of stability of the power supply.

Calibration of amplifier gain settings with the entire electronic system in operation was done by applying pulses from a RIDL Model 47-4A mercury pulser to the Tennelec 100B preamplifier with the counter connected in normal operation. The height of the pulse from the mercury pulser was measured with a Keithley microvoltmeter. This is a reasonably accurate null-deflection method which measures non-linearities in the system. This measurement of non-linearity is important for the fitting of the M-spectrum to the L-spectrum, which must be measured in separate runs, as explained below.

The lower level discriminator of the 128-channel analyzer was set

in order to place the zero-energy point in a low positive channel and also to avoid noise pulses. The discrimination level of the paralysis pulse generator was set at a level corresponding to the mean energy of the M spectrum (~ 17 eV). The input to the analyzer, together with the paralysis pulse, was displayed continuously on an oscilloscope so that the complete system could be inspected for proper operation during the runs.

All of these electronic checks, such as the determination of the analyzer zero-point and non-linearity, of the discrimination levels for the analyzer and the paralysis pulse generator, of the pedestal of the linear anticoincidence gate, and of the gain stability, were made before and after each run.

Experimental Measurements

In order to determine the optimum paralysis time for these experiments, a series of runs was done in which M-spectra of Ar^{37} were compared as a function of paralysis pulse width from zero to 8.5 milliseconds.

In Figure 8, the M-spectrum of Ar^{37} is shown as a function of paralysis pulse width. No significant difference in the spectrum was observed with paralysis times longer than about 700 microseconds with a fresh Ar^{37} source (less than two months after the end of the reactor irradiation). As the source aged (up to one year after irradiation with storage over Na-Pb alloy at room temperature), a gradual increase in this minimum paralysis time was found to be necessary, up to about two milliseconds. This suggests that the concentration of electron-attaching impurities (oxygen, moisture) gradually increased, as the source aged, in spite of the presence of sodium-lead alloy. Therefore, all further ex-

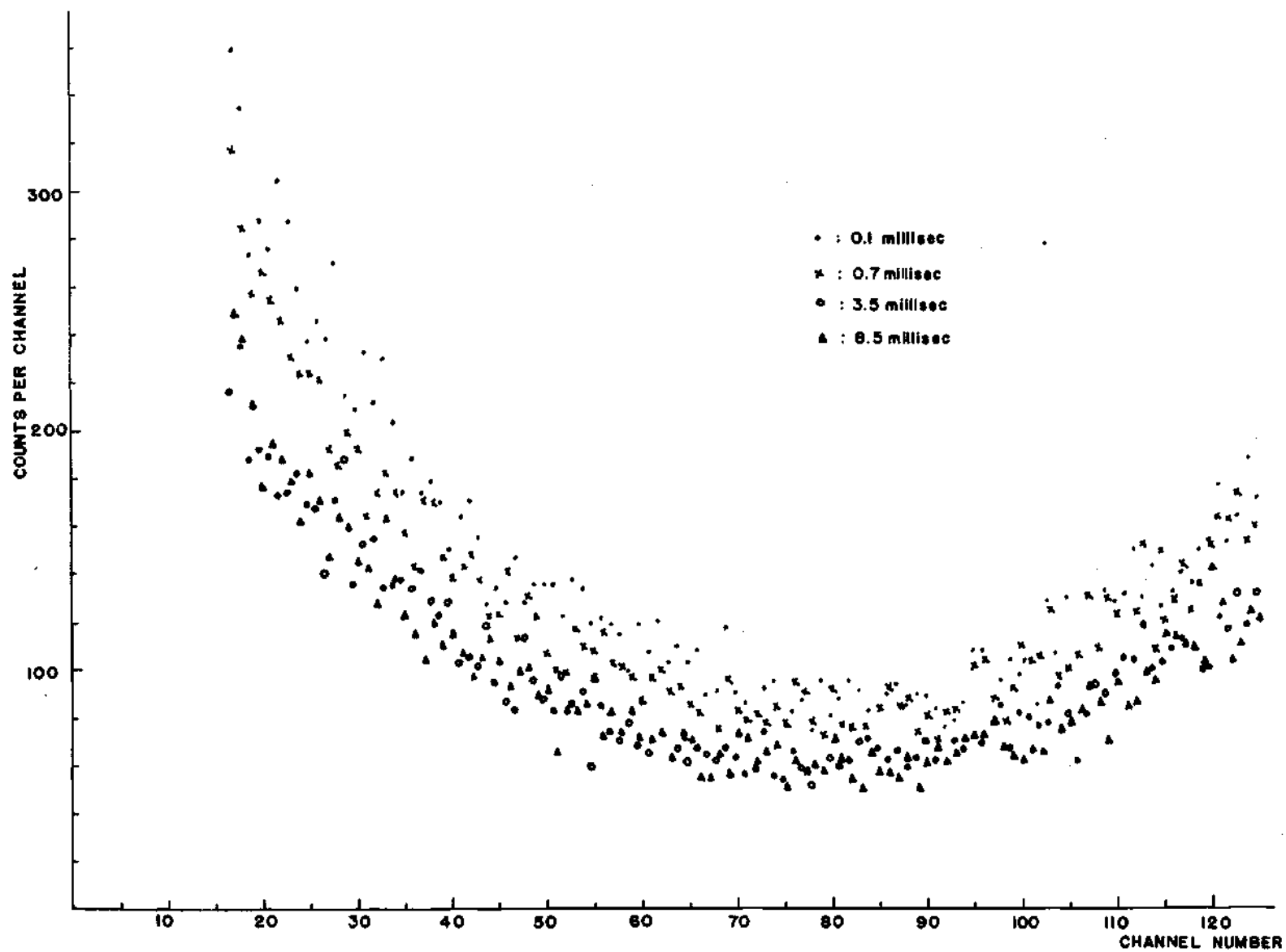


Figure 8. Ar^{37} M-spectrum as a Function of Paralysis Pulse Width

periments on Ar^{37} were run with a paralysis time of 3.8 milliseconds, in order to assure that the M-spectrum was independent of effects due to negative ion formation and afterpulses.

The sequence of operations in a typical run to measure the M-, L-, and K-spectra in Ar^{37} decay is discussed below.

The M-, L-, and K-spectra were taken in separate runs at the same gas gain ($\sim 10^4$) but with different electronic gains of 256, 38.4, and 4.0, respectively. The total gain per primary electron was, respectively, 2.56×10^6 , 3.8×10^6 , and 4.0×10^6 . The total gain per primary electron was not kept constant, but for the L- and M-spectra was put in the ratio 3.8/2.56 in order to overlap the upper part of the M-spectrum with the lower part of the L-spectrum and thus to fit the two spectra into a composite one for measurement of the intensity ratio (areas), N_M/N_L . (The M-, L-, and K-spectra must be taken separately in order to expand these regions of interest over the limited 10 volt range of the 128-channel analyzer.)

A typical run involved the following sequence: calibration (as discussed above beginning on page 29); measurement of the Ar^{37} K-spectrum for 30 minutes; measurement of the M-spectrum for three hours; again a 30 minute K-spectrum; a single-electron spectrum with ultraviolet photons for 10 minutes with subtraction of a 10 minute M-spectrum to get the net single-electron spectral shape; further accumulation of the M-spectrum for four hours; measurement of the L-spectrum for three hours; followed by calibrations (see page 29).

Runs were made at one and two atmospheres absolute counter pressure, in order to vary the K x-ray escape, which is a critical correction

(see page 39).

The background of the counter, inside five cm of lead shielding, was determined by refilling with the same gas mixture and pressure, but omitting the Ar^{37} source. The 5.9 keV K x-rays of Fe^{55} were used externally to recalibrate background runs for the same gas gain as used in the K-, L-, M-spectral regions in the Ar^{37} measurements.

Results of typical runs are shown in Figures 9 (K-spectrum), 10 (M + L composite spectrum), and 11 (M-spectrum, together with single-electron shape and background). After many preliminary trials, five complete runs at one atmosphere absolute pressure and two complete runs at two atmospheres were made to obtain the present results, based on two different irradiated sources of Ar^{37} .

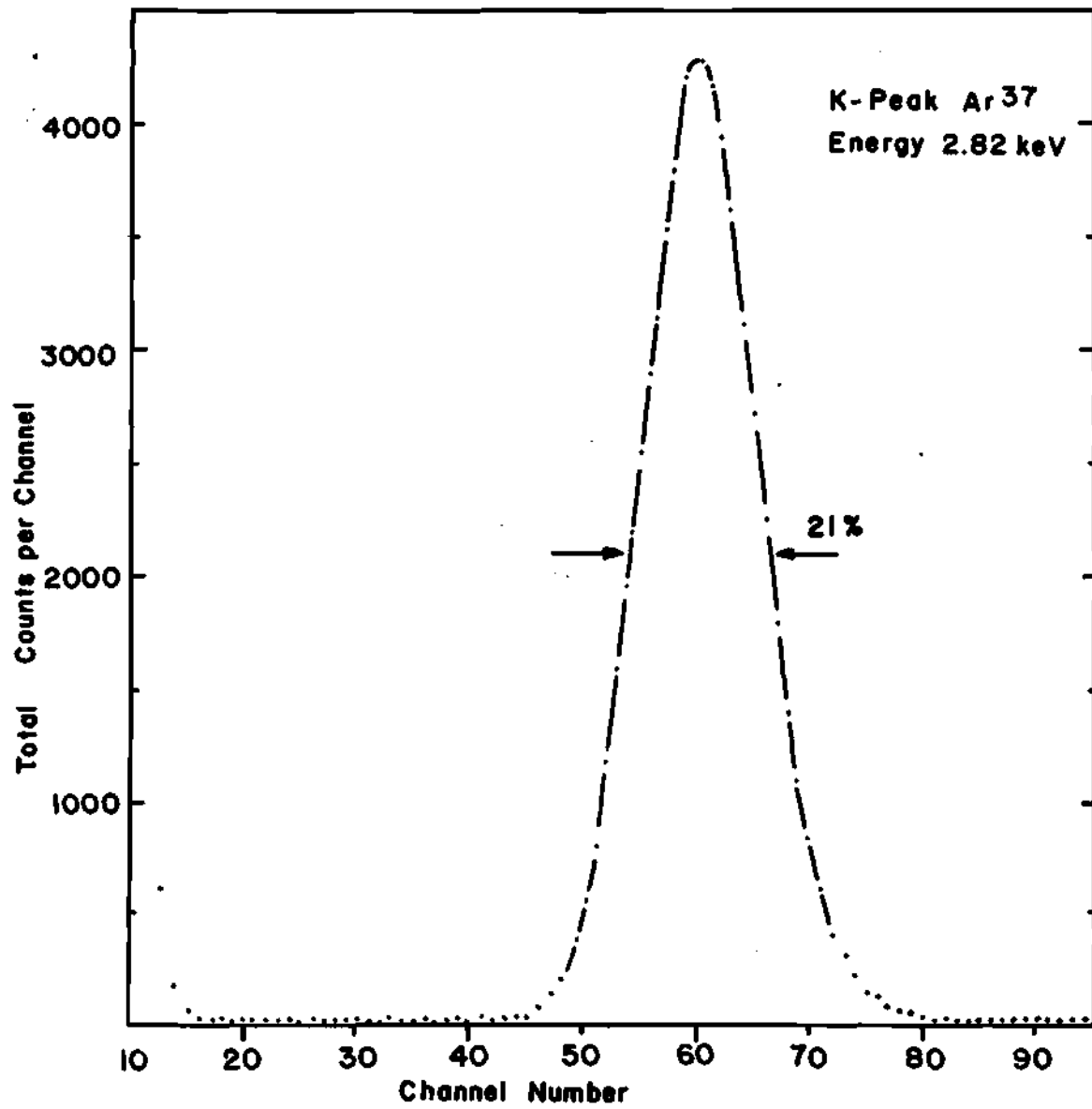


Figure 9. Spectrum of Ar³⁷ K-peak

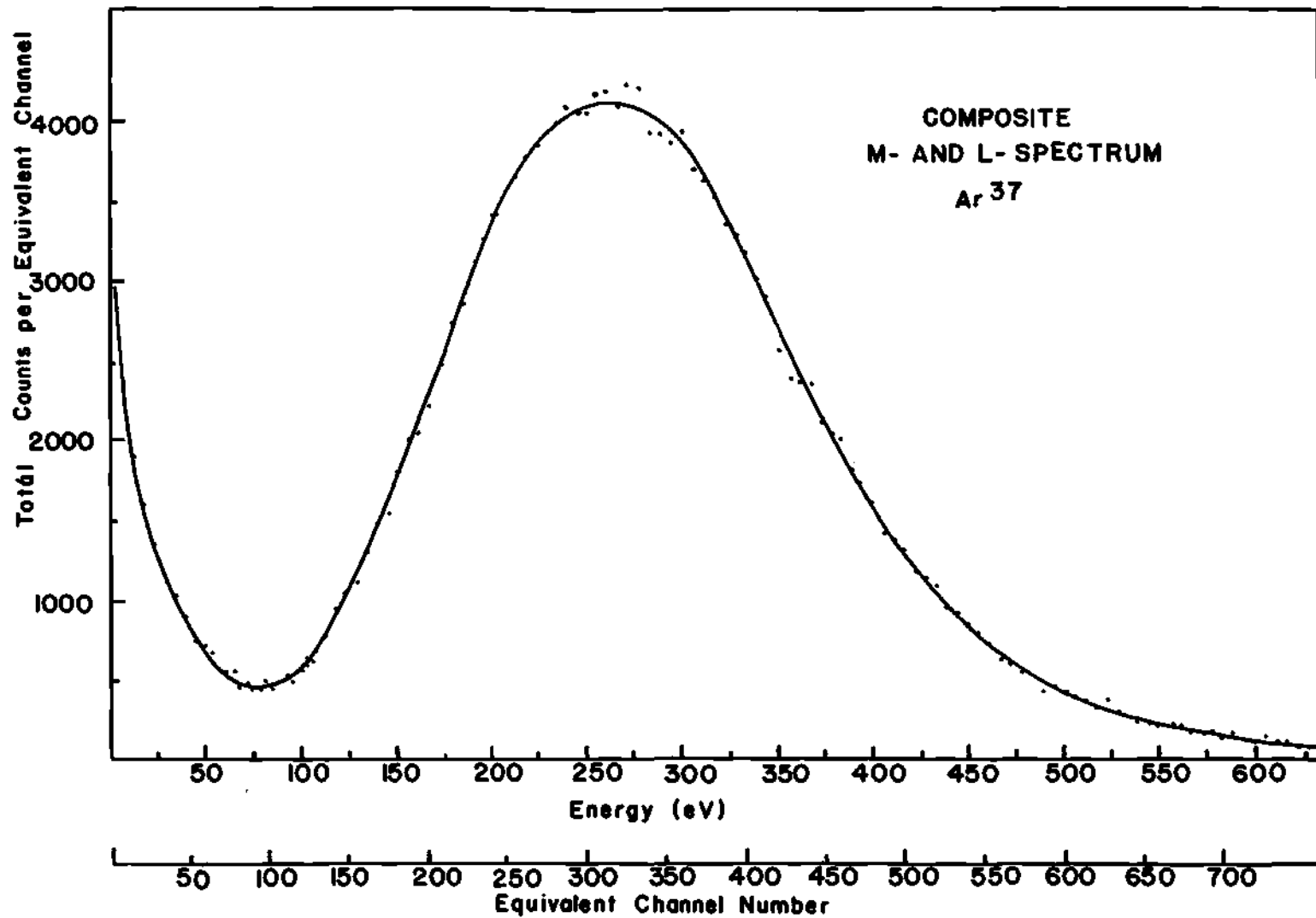


Figure 10. Ar³⁷ M + L Composite Spectrum and Background Shape

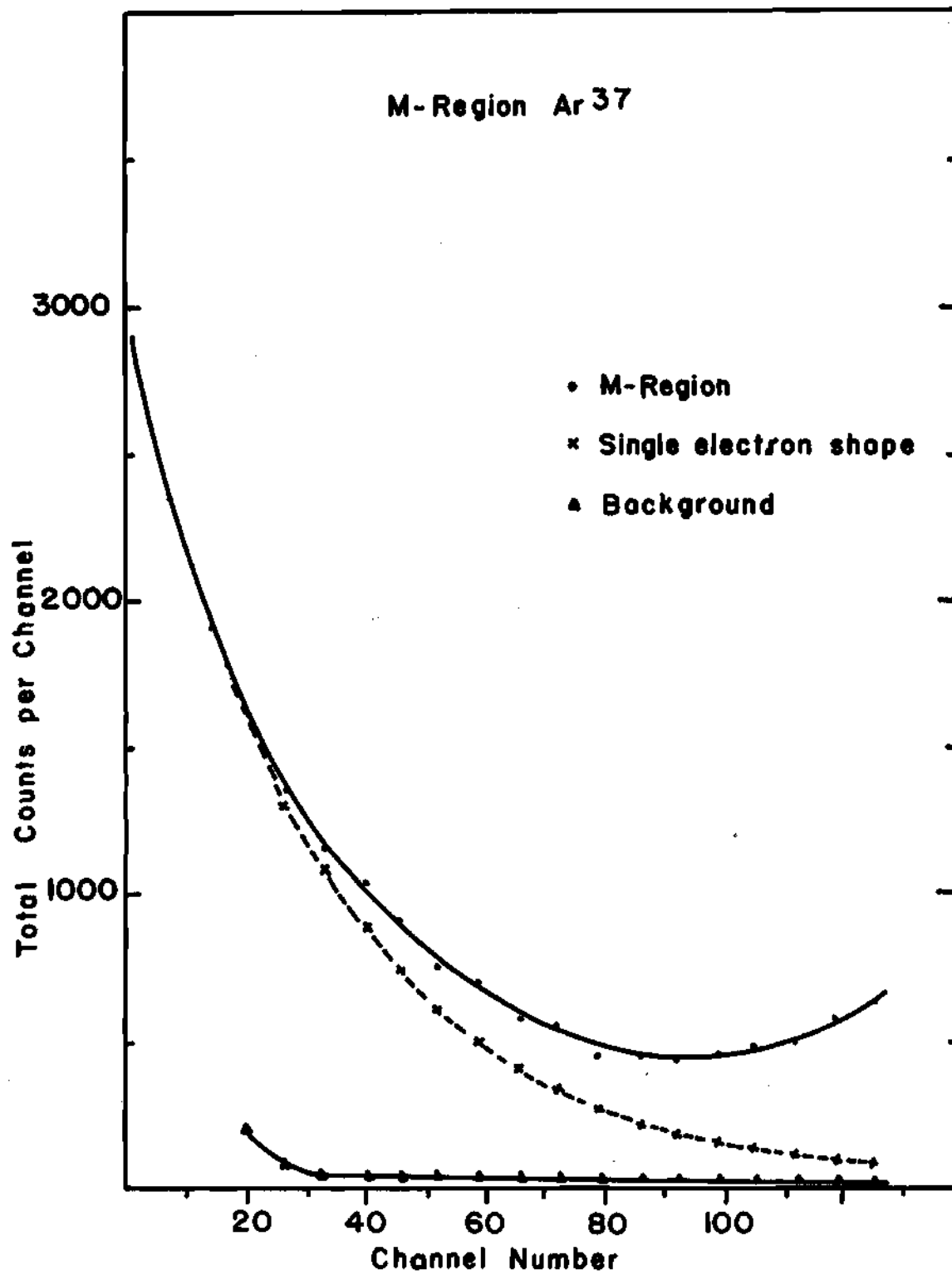


Figure 11. Ar³⁷ M-spectrum with Single-electron Shape and Background Spectrum

CHAPTER III

RESULTS

Data and Computation of Observed L/K and M/L Intensity Ratios

From a precise knowledge of the gain ratio between the M- and L-spectra, the M- and L-spectra were fitted together into a composite spectrum having equalized channel widths for the M- and L- regions, as shown in Figure 10. A check of the goodness of the fit in the region of overlap between the M- and L-spectra was obtained from the fact that the intensities of the M-points and the L-points matched in the overlap region (Figure 10).

To separate the contributions from M- and L-events in the region of overlap, the single-electron spectrum (from ultraviolet photons) was fitted at channels 17 to 22 in the M-region, Figure 10, where the contribution due to L-events is negligible. Following the criteria of Gold and Bennett (21) for the proper shape of a single-electron spectrum, the fitting was not carried below about channel 17.

All fitting of spectra described above was done after background subtraction, which was quite small. A typical background counting rate in the M-region at one atmosphere was about seven counts/channel per hour, (Figure 10).

Using this gain calibration, the area under the fitted single-electron spectrum represented the number of M-events counted, and the difference between the total M-spectrum and the fitted single-electron

spectrum was ascribed to L-events. All the spectra were corrected for deadtime due to the paralysis pulse generator.

After subtraction of background, the region between the K-peak (2822 eV) and the L-peak (265 + 10 eV) exhibited a constant residual intensity, probably due to the degradation of K-events in the counter.* This low energy tail from the K-peak has been extrapolated linearly to zero energy. It contributes an uncertainty in the final M/L intensity ratio of about eight percent.

The ratio of areas under the net corrected M- and L-spectra, N_M/N_L , is the observed M/L intensity ratio, uncorrected for K x-ray escape. Values of N_M/N_L for the seven final runs are given in Table 1.

In the same manner, the ratio of areas under the L-peak and K-peak, N_L/N_K , is the observed L/K intensity ratio, uncorrected for K x-ray escape.

Correction for K X-ray Escape and Calculation of Final Results

The values obtained, Table 1, for N_L/N_K and N_M/N_L must be corrected for K x-ray escape for the following reason. When a K_{α} x-ray escapes detection entirely, the primary K-shell vacancy appears in the L-shell, and

*The degradation of a very small fraction of the total K-events is thought to arise from secondary electrons ejected from the aluminum walls when K x-rays strike the walls and from K x-rays which escape in part from the sensitive volume into the insensitive end-zones of the counter, where the field-adjusting tubes cut off the gas multiplication; or from the end-zones into the sensitive volume.

Another possible contribution to the degradation arises from possible losses of optical photons, from the electron avalanche, which do not produce single-electrons and so constitute an uncompensated energy loss. Since all these degradation effects are random in energy, this would give rise to a constant intensity energy distribution below the K-peak.

Table 1. Observed M/L Intensity Ratios, Uncorrected for K X-ray Escape

Run No.	Counter Pressure (Atmos.)	K-peak Resolution (% FWHM)	K-peak to Valley Ratio (Background subtracted)	L-peak Resolution (% FWHM)	L-peak to Valley Ratio (Between M and L regions)	N_L/N_K	N_M/N_L
1	1	21	337 :1	80	9.5 :1	0.150	0.075
2	1	21	240 :1	80	9.0 :1	0.153	0.070
3	1	21	242 :1	80	9.1 :1	0.154	0.071
4	1	21	239 :1	80	9.0 :1	0.153	0.072
5	1	21	245 :1	80	9.2 :1	0.154	0.069
6	2	21	335 :1	81.6	8.45:1	0.131	0.086
7	2	21	339.1:1	81.0	8.9 :1	0.132	0.088

the event will be registered in the L-peak; similarly, when a K_{β} x-ray escapes, the primary K vacancy appears in the M-shell, and the event will be registered in the M-spectrum. The detection efficiency is essentially 100 percent for L and M x-rays and Auger electrons; thus, the escape of L and M events in these experiments is taken to be zero.

Owing to the fact that there are some 10 times more K-captures than L-captures, and some 10 times more L-captures than M-captures, even a small fraction of K x-ray escape gives rise to an appreciable correction in the L- and M-intensities. This correction, in turn, depends critically on the value of the K-fluorescence yield, ω_K (33) of the daughter atom (chlorine) and on the probability, P, for escape of K x-rays without detection, from the counter (12).

The results were calculated by means of the following quantitative relationships. The observed number of events in the M-spectrum is given by:

$$N_M = P_M + (\omega_K P) P_K k_{\beta} \quad (9)$$

and the observed number of events in the L-peak is given by:

$$N_L = P_L + (\omega_K P) P_K k_{\alpha} \quad (10)$$

The observed number of events in the K-peak is

$$N_K = P_K - (\omega_K P) P_K (k_{\alpha} + k_{\beta}) \quad (11)$$

where $k_{\alpha} + k_{\beta} = 1$

k_{α} = fraction of K_{α} x-rays in the K x-ray series for the daughter atom (chlorine, $Z = 17$)

k_{β} = fraction of K_{β} x-rays in the K x-ray series of the daughter atom

P_M , P_L , and P_K are the respective probabilities of orbital electron capture from the M-, L-, and K-shells occurring in the sensitive volume of the counter.

The above equations are based on the assumption that no escape of K Auger electrons or of L- or M-events occurs. The only escape is due to K x-rays.

Dividing the ratio of equations 10 and 11 by P_K , one obtains

$$\left(\frac{N_L}{N_K} \right) - \left(\frac{P_L}{P_K} \right) = (\omega_K P) \left[\frac{N_L}{N_K} + k_{\alpha} \right] \quad (12)$$

from which

$$(\omega_K P) = \frac{(N_L/N_K) - (P_L/P_K)}{[(N_L/N_K) + k_{\alpha}]} \quad (13)$$

which is the fraction of K x-rays which escapes detection entirely.

The observed M/L intensity ratio, from equations 9 and 10 is

$$\left(\frac{N_M}{N_L} \right) = \frac{P_M + (\omega_K P) P_K k_{\beta}}{P_L + (\omega_K P) P_K k_{\alpha}} \quad (14)$$

Dividing equation 14 by P_L , one obtains

$$\left(\frac{N_M}{N_L}\right) = \frac{(P_M/P_L) + (P_K/P_L) k_\beta (\omega_K P)}{1 + (P_K/P_L) k_\alpha (\omega_K P)} \quad (15)$$

and rearranging equation 15, one obtains

$$(P_M/P_L) = (N_M/N_L) \left[1 + \frac{(\omega_K P) k_\alpha}{P_L/P_K} - \frac{(\omega_K P) k_\beta}{(P_L/P_K)(N_M/N_L)} \right] \quad (16)$$

where the quantity $(\omega_K P)$, the fraction of K x-ray escape, is obtained from equation 13 as a function of k_α , from the experimental measurement of the (N_L/N_K) ratio and a value of $(P_L/P_K) = 0.102 \pm 0.003$ from precision measurements summarized in the literature (16). Substituting equation 13 for $(\omega_K P)$ into equation 16 gives

$$(P_M/P_L) = (N_M/N_L) \left[1 + \frac{k_\alpha}{(P_L/P_K)} \cdot \frac{(N_L/N_K) - (P_L/P_K)}{(N_L/N_K) + k_\alpha} \right. \\ \left. - \frac{(1 - k_\alpha)}{(P_L/P_K)(N_M/N_L)} \cdot \frac{(N_L/N_K) - (P_L/P_K)}{(N_L/N_K) + k_\alpha} \right] \quad (17)$$

The final values of the M/L orbital electron capture ratio, P_M/P_L , are computed from equation 17. Typical numerical evaluation of equation 17 is, for an average of the runs at one atmosphere,

$$(P_M/P_L) = 0.0714 \left[1 + \frac{k_\alpha}{0.102} \frac{0.153 - 0.102}{0.153 + k_\alpha} \right] \quad (18)$$

$$- \left[\frac{1 - k_{\alpha}}{(0.102)(0.0714)} \frac{0.153 - 0.102}{0.153 + k_{\alpha}} \right]$$

which reduces to the following relationship (for the runs at one atmosphere)

$$(P_M/P_L) = 0.0714 + 0.500 \left[\frac{1.0714 k_{\alpha} - 1}{k_{\alpha} + 0.153} \right] \quad (19)$$

From equation 19, it can be seen that the corrected capture ratio, P_M/P_L , is a sensitive function of k_{α} , the fraction of K_{α} x-rays in the K x-ray series of chlorine ($Z = 17$), for single-wire counter experiments having substantial escape of K x-rays. In this example, (P_M/P_L) varies by about 95 percent, from a value of 0.0367 to 0.1024, as k_{α} varies by about 14 percent, from a value of 0.87 to 1.00.

In the case of the runs carried out at two atmospheres pressure, equation 17 becomes

$$(P_M/P_L) = 0.087 + 0.289 \left[\frac{1.087 k_{\alpha} - 1}{k_{\alpha} + 0.1315} \right] \quad (20)$$

in which case, (P_M/P_L) varies from 0.0713 to 0.1092, as k_{α} varies from 0.87 to 1.00.

The final evaluation of P_M/P_L must be expressed, as in equations 19 and 20, in terms of k_{α} because no values of k_{α} are known below $Z = 23$ (35, 36).

In order to discuss the significance of the results, equations 19 and 20, the experimental errors must be taken into account. In any case, it is clear that, owing to the sensitive dependence of (P_M/P_L) on k_α , a measurement of (P_M/P_L) to ± 8 percent, as discussed below, would determine the value of k_α for chlorine ($Z = 17$) to better than one percent.

Evaluation of Experimental Errors

One of the principal errors in this result is due to the fitting of a single electron spectrum to the M-shape. This amounts to about ± 5 percent. The fact that the spectrum has to be extrapolated to zero energy, due to the necessity of biasing the first six channels to eliminate noise, contributes an uncertainty of ± 6 percent. (A possible reduction in the error due to zero energy extrapolation might be realized by additional measurements using single electron spectra at different gas gains.) The statistical uncertainty contributes about ± 3 percent.

The main error, however, is a systematic one. It is due to the fact that there appears to be an energy loss from the K-peak. The low energy tail from the K-peak, which might arise from degraded K-events (see footnote, page 39), has been extrapolated linearly to zero energy. This is unlikely to exceed a maximum contribution to the error of about eight percent. Consequently, the total error in the experimental values of N_M/N_L (Table 1) lies within ± 9 percent, and in the experimental values of N_L/N_K , within ± 1.4 percent.

Experimental factors which can cause the observed M/L intensity ratio to be too high, such as negative ion formation and/or clipping of large pulses into small ones by the electronics, have been eliminated as

discussed in Chapter II.

A phenomenon that conceivably could cause the experimental M/L intensity ratio to appear to be too low might be Coster-Kronig transitions in the M-shell (33). By this is meant that, for example, a primary vacancy in the M_1 subshell of chlorine [binding energy $\cong 17.5$ eV (32)] might be shifted to a higher M-subshell, such as $M_{4,5}$ [binding energy \sim a few eV (unknown)] with emission of the binding energy difference in the form of an ultraviolet photon. Such ultraviolet photons could be absorbed by the quenching gas (propane) without creating an electron. Any such process would result in an M-capture event that fails to produce a single primary electron and, therefore, would not be detected.

However, this is a negligible process for the M-shell in chlorine ($Z = 17$) for the following reason. The binding energy difference, for example in the M_1 - $M_{4,5}$ Coster-Kronig transition, is much more likely to appear as kinetic energy of an ejected $M_{4,5}$ electron in a radiationless transition. As Snell points out (37), radiationless transitions are favored in low-Z elements and always dominate in the M, N, and higher shells for the ordinary Auger effect (e.g., K-L-M-N-transitions). Since Coster-Kronig transitions differ from ordinary Auger transitions only in that the vacancies are shifted within the same shell, the probability that the Coster-Kronig transition will be radiationless is essentially unity, because of the very low transition energies.

Consequently, in the present experiment, it is likely that radiative Coster-Kronig transitions in the M-shell of chlorine are entirely negligible and do not affect the present results.

The Capture Ratio, P_M/P_L , as a Function of k_α

The capture ratio, P_M/P_L , as a function of k_α , from equations 19 and 20, for runs at one atmosphere and two atmospheres, respectively, is plotted in Figure 12, in which the error limits have been included. From this figure, it is seen that the one atmosphere and two atmosphere results for P_M/P_L versus k_α overlap only for values of $k_\alpha > 0.95$ for $Z = 17$, and, therefore, the P_M/P_L ratio is restricted between the extreme values

$$0.085 \leq P_M/P_L \leq 0.110$$

representing the largest possible spread with maximum error limits included. The most probable values of P_M/P_L lie in the region of

$$0.085 \leq P_M/P_L \leq 0.105$$

From Figure 12, it is also seen that a better measurement of P_M/P_L and k_α can be obtained by making runs at a lower pressure, to get a more vertical line, and at higher pressure and/or with krypton gas instead of argon as counter gas, to get a more horizontal line.*

* Additional runs at various pressures and with krypton-propane gas fillings are in progress by H. D. Genz and J-P. A. Renier.

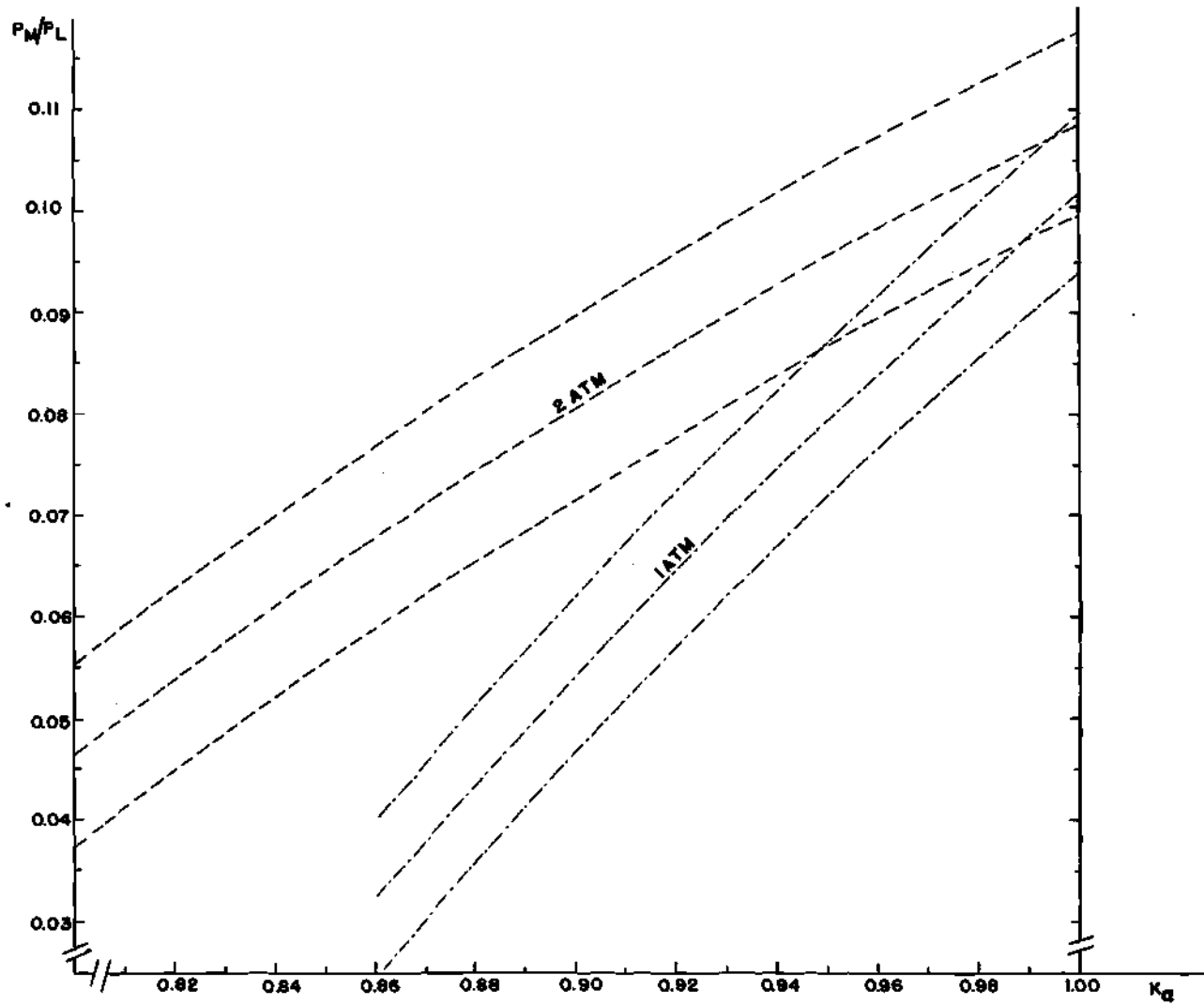


Figure 12. Plot of (P_M/P_L) Capture Ratio versus k_α

CHAPTER IV

DISCUSSION OF RESULTS

The result of the present experiments, $P_M/P_L = 0.085$ to 0.105 , has been plotted in Figure 1, point (a). The theory with exchange (10) for Ar^{37} decay predicts a value of $(P_M/P_L) = 0.128 \pm 0.0026$, which is in clear disagreement with even the upper limit of the present results. The theory without exchange (10) predicts $(P_M/P_L)^0 = 0.0976 \pm 0.001$, which overlaps slightly with the upper limit of the present result (see Figure 1). Curve A in Figure 1 is based on old hydrogen-like wave functions with Slater screening (9), and it predicts a value of the M/L ratio of about 0.034, which is definitely ruled out by present results.

In spite of the slight agreement of the upper limit of the present result with the theoretical value of Bahcall (10) without exchange, any theory of M-capture probability which fails to take account of exchange-overlap effects cannot be taken rigorously, in view of the fact that for L-capture the exchange correction has been thoroughly established experimentally (6,13,16), and the predicted (10) exchange-overlap correction, $X^{M/L}$, is even larger for M-capture than for L-capture.

The disagreement of M/L capture ratios with exchange-corrected Hartree-Fock wave function theory (10) appears to be much larger (Figure 1) than in the case of L/K capture ratios (6). This suggests that the origin of these disagreements might lie with the screening assumptions made in derivation of the Hartree-Fock wave functions of Watson and Free-

man (11).

As pointed out in the Introduction, several new calculations of accurate analytical SCF Hartree-Fock wave functions for the low-Z region have been very recently reported (23, 24, 25). It remains to be shown whether these new Hartree-Fock wave functions, evaluated at the nucleus, will bring the theoretical L/K and M/L orbital electron capture ratios into closer agreement with experiment.

BIBLIOGRAPHY*

1. W. M. Hubbard, "M-shell Electron Capture Contribution to Orbital Electron Capture," Phys. Rev. 137, B245 (1965); and Ph.D. Thesis, "Theoretical Considerations of the Contribution of M-shell Electrons to Orbital Electron Capture," Georgia Institute of Technology (1962).
2. R. E. Marshak, "Forbidden Transitions in β -decay and Orbital Electron Capture and Spins of Nuclei," Phys. Rev. 61, 431 (1942).
3. E. Segré, "Possibility of Altering the Decay Rate of a Radioactive Substance," Phys. Rev. 71, 274 (1947).
4. R. Bouchez, R. Daudel, P. Daudel, and R. Mauxart, "Variation de la Période du Nuclide Be^7 en fonction du degré d'ionisation de l'atome," Compt. rend. 227, 525 (1948); J. Phys. Radium 8, 336 (1948).
5. H. Brysk and M. E. Rose, "Theoretical Results on Orbital Capture," Oak Ridge Report ORNL-1830 (1955) (Unpublished) and Revs. Modern Phys. 30, 395 (1958).
6. G. Winter, "Revised L_1/K Theoretical Calculations for Allowed Transitions," Ann. Physik (Leipzig), in press (1966); Preprint (1966).
7. B. L. Robinson, "Capture of Outer Orbital Electrons," Nuclear Phys. 64, 197 (1965).
8. H. R. Brewer, D. S. Harmer, and D. H. Hay, "M-shell, Relativistic Electron Wave Functions," Phys. Rev. Lett. 7, 319 (1961).
9. A. H. Wapstra and W. Van der Eijk, "The Decay of Cd-109, Ag-109, and Pd-109," Nuclear Phys. 4, 325 (1957).
10. J. N. Bahcall, "Effect of Exchange on M/L-Electron Capture Ratios," Phys. Rev. 131, 1756 (1963).
11. R. E. Watson and A. J. Freeman, "Analytical Hartree-Fock Wave Functions for the 3p-shell Atoms," Phys. Rev. 123, 521 (1961); 124, 1117 (1961).

*The abbreviations used herein follow the American Physical Society Style Manual.

BIBLIOGRAPHY (Continued)

12. B. L. Robinson and R. W. Fink, "L/K-Capture Ratios, Transition Energies, and Mean L-fluorescence Yields in Orbital Electron Capture," *Revs. Modern Phys.* 27, 424 (1955); "Recent Experimental Results on Orbital Electron Capture," *Revs. Modern Phys.* 32, 117 (1960).
13. R. Bouchez and P. Depommier, "Orbital Electron Capture by the Nucleus," *Proc. Conf. on Atomic Electrons in Nuclear Transformations*, I, 30 (1963), Warsaw, Poland; and *Rept. Prog. Phys.* 23, 395 (1960).
14. J. N. Bahcall, "Effect of Exchange on L to K Capture Ratios," *Phys. Rev. Lett.* 9, 500 (1962); "Exchange and Overlap Effects in Electron Capture and in Related Phenomena," *Phys. Rev.* 132, 362 (1963); "Overlap and Exchange Effects in Beta-Decay," *Phys. Rev.* 132, 362 (1963); 129, 2683 (1963).
15. S. Odier and R. Daudel, "Contribution à l'étude de la Capture des Electrons du Cortège par les noyaux d'atomes: effet des corrélations existant entre les positions des électrons sur le rapport de la probabilité de capture L à celle de capture K," *J. Phys. Radium* 17, 60 (1956).
16. R. W. Fink, "Comparison with Theory of Experimental Values of L/K-Capture Ratios for Allowed and First-forbidden Transitions," U. S. Atomic Energy Commission Report, ORO-3346-8(rev) (1966) (Unpublished).
17. R. W. Fink and K. W. D. Ledingham, "Comparison of Allowed M/L Orbital Electron Capture Ratios with Theory," *Bull. Am. Phys. Soc.* 11, No. 3, 352 (1966) and Preprint (Unpublished).
18. J. H. E. Mattauch, W. Thiele, and A. H. Wapstra, "1964 Atomic Mass Table," *Nuclear Phys.* 67, 1 (1965).
19. P. W. Dougan, K. W. D. Ledingham, and R. W. P. Drever, "The L/K Capture Ratio of Ar-37," *Phil. Mag.* 7, 475 (1962).
20. A. P. Lukirskii, O. A. Ershov, and I. A. Brytov, *Bull. Acad. Sci., USSR, Phys.* 27, 447, 798 (1963) [*Izv. Akad. Nauk SSSR, Ser. Fiz.* 27, 446, 798 (1963)], "Proportional Counters for Soft X-rays," "Operation of Proportional Counters in the Ultra-soft X-ray Region."
21. R. Gold and E. F. Bennett, "Electron Multiplication Process in Proportional Counters," *Phys. Rev.* 147, 201 (1966); see also N. Spielberg, "Multiplication Process in Proportional Counters," *Bull. Am. Phys. Soc.* 12, 288 (1967); *Rev. Sci. Instr.* 37, 1268 (1966).

BIBLIOGRAPHY (Continued)

22. J. L. Campbell and K. W. D. Ledingham, "Pulse Height Distributions from Proportional Counters," *Brit. J. Appl. Phys.* 17, 769 (1966).
23. G. L. Malli, "Accurate Analytical Self-Consistent Field Hartree-Fock Wave Functions for Second-Row Atoms," *Can. J. Phys.* 44, 3121 (1966); and G. Malli and S. Fraga, "Charge Densities at the Nucleus," *Can. J. Phys.* 44, 3131 (1966).
24. E. Clementi, "Analytical Self-Consistent Field Functions for Positive Ions. II. Iso-electronic Series with 11 to 18 Electrons," *J. Chem. Phys.* 38, 1001 (1964); 41, 295 (1964); "Tables of Atomic Functions," IBM Corp. (San Jose, Calif.) (Unpublished) (1965).
25. P. S. Bagus, Unpublished Results, Argonne National Laboratory (1964).
26. R. W. P. Drever, private communication (1965).
27. P. W. Dougan, K. W. D. Ledingham, and R. W. P. Drever, "The Decay of Cl-36 to S-36," *Phil. Mag.* 7, 1223 (1962).
28. H. Weiss and E. Masanz, "An Indicating Circuit for Afterpulses in Geiger-Müller Counters," *Atomkernenergie* 11, 489 (1966).
29. S. C. Curran, A. L. Cockcroft, and J. Angus, "Investigation of Soft Radiation by Proportional Counters - Use as a Detector of Ultra-violet Quanta and Analysis of the Gas Multiplication Process," *Phil. Mag.* 40, 929 (1949).
30. H. S. Snyder, "Fluctuations in Proportional Counters," *Phys. Rev.* 72, 181 (1947); and O. R. Frisch, Atomic Energy of Canada, Ltd. Report CRL-57 (1959) (Unpublished).
31. G. C. Hanna, D. H. W. Kirkwood, and B. Pontecorvo, "High Multiplication Proportional Counters for Energy Measurements," *Phys. Rev.* 75, 985 (1949).
32. J. A. Bearden and A. F. Burr, "Reevaluation of X-ray Atomic Energy Levels," *Rev. Modern Phys.* 39, 125 (1967).
33. R. W. Fink, R. C. Jopson, Hans Mark, and C. D. Swift, "Atomic Fluorescence Yields," *Revs. Modern Phys.* 38, 513 (1966).
34. C. Manduchi and G. Zannoni, "Measurement of the M/L-Capture Ratio in Ge⁷¹ Decay," *Nuovo cim.* 24, 181 (1962); *Nuclear Phys.* 36, 497 (1962).

BIBLIOGRAPHY (Concluded)

35. J. H. Williams, "Relative Intensities and Transition Probabilities of the K-Series Lines of the Elements 24 to 52 by the Ionization Chamber Method," *Phys. Rev.* 44, 146 (1933); and H. T. Meyers, *Wiss. Verh. Siemens Labor.* 7, 108 (1929) as given by A. H. Wapstra, G. J. Nijgh, and R. Van Lieshout, Nuclear Spectroscopy Tables (North-Holland Publishing Co., Amsterdam, 1959), p. 81.
36. S. I. Salem and J. P. Johnson, " M_3 -K and L_3 -K Transition Probability," *Bull. Am. Phys. Soc.* 11, 914 (1966); and private communication (January, 1967).
37. A. H. Snell, "Atomic and Molecular Consequences of Radioactive Decay," in K. Siegbahn, Ed., Alpha-, Beta-, and Gamma-Spectroscopy (North-Holland Publishing Co., Amsterdam, 1964), pp. 1545 ff.
38. P. W. Dougan and R. W. P. Drever, Unpublished Studies, 1959, quoted in K. W. D. Ledingham Thesis (1963).
39. G. Winter, private communication (1966).
40. R. B. Moler and R. W. Fink, " M/L - and L/K -Orbital Electron Capture Ratios and Transition Energy in Cd^{109} Decay," *Phys. Rev.* 139, B282 (1965).
41. H. Lentz, K. Schneckenberger, and H. Wenninger, "Electron Capture Ratios in Cd^{109} . . .," *Nuclear Phys.* 63, 263 (1965).
42. C. Manduchi, G. Nardelli, M. T. Russo-Manduchi, and G. Zannoni, "On the Decay of Sn^{113} ," *Nuovo cim.* 33, 49 (1964); 31, 1380 (1964).
43. G. Winter, private communication (1966); G. Winter, K. Hohmuth, and J. Schintlmeister, "Das M/L Einfanzverhältnis von Xe^{127} ," *Nuclear Phys.* 73, 191 (1965).
44. H. Lentz, G. Schulz, and H. Wenninger, "Electron Capture Ratios in the Decay of Tl^{202} ," *Nuclear Phys.* 75, 81 (1966).
45. G. Schulz, Heidelberg, private communication (1967).